Maintenance of convectively coupled Kelvin waves: relative importance of internal thermodynamic feedback and external momentum forcing

Mu-Ting Chien[1], Daehyun Kim[2,3], & Patrick Haertel[4]

1Department of Atmospheric Science, Colorado State University

2Department of Atmospheric and Climate Sciences, University of Washington

3School of Earth and Environmental Sciences, Seoul National University, South Korea

4School of Earth and Planetary Sciences, Yale University

E-mail: muting.climate.science@gmail.com

Under review in a peer-reviewed journal *Geophysics Research Letters, resubmitted on May 21, 2025*

Maintenance of Convectively Coupled Kelvin Waves: Relative Importance of Internal Thermodynamic Feedback and External Momentum Forcing

Mu-Ting Chien[1,2], Daehyun Kim[1,3*], & Patrick Haertel[4]

[1]Department of Atmospheric and Climate Science, University of Washington

[2]Department of Atmospheric Science, Colorado State University

[3]School of Earth and Environmental Sciences, Seoul National University, South Korea

[4]Department of Earth and Planetary Sciences, Yale University

*Corresponding author: Daehyun Kim (daehyun@snu.ac.kr)

Key Points:

- Convectively coupled Kelvin waves (KWs) are maintained primarily by the internal thermodynamic feedback in all regions and seasons.
- The internal thermodynamic feedback is the most dominant over the warmest ocean, with the weakest mean westerly aloft.
- The observed relative importance of the two maintenance processes serves as a reference for evaluating KWs in numerical simulations.

Abstract

Previous studies suggest that convectively coupled Kelvin waves (KWs) are likely maintained by two distinct processes: (1) the internal thermodynamic feedback between KW diabatic heating and temperature and (2) the external momentum forcing from the midlatitude Rossby waves exerting on KW zonal wind. This study quantifies the relative importance of the two processes on KW maintenance by comparing the growth rates of eddy available potential energy (EAPE) and eddy kinetic energy (EKE) within KWs using satellite and reanalysis data. Results show KWs are maintained primarily by the internal thermodynamic feedback in all regions and seasons, especially over the Indian Ocean, where the mean state sea surface temperature is the highest, and the upper tropospheric westerly is the weakest. Overall, the observed relative importance of the two maintenance processes can serve as a reference for numerical simulations of KWs.

Plain Language Summary

Convectively coupled Kelvin waves (KWs) generate regions of enhanced and suppressed thunderstorms that move eastward along the equator. These waves occur periodically with a 5-6-day timescale with particular zonal wind and temperature structures. KWs persist primarily because of certain mechanisms that enhance and sustain them. These mechanisms can be summarized into two distinct processes: (1) the positive feedback between KW temperature and diabatic heating from the cloud processes or (2) the zonal momentum forcing, which originates from the midlatitudes remotely amplifies the zonal wind of KWs. By quantifying the relative importance of the two maintenance processes, we found that the first mechanism is the most dominant across the entire tropics.

1 Introduction

Convectively coupled Kelvin waves (KWs) contribute significantly to tropical precipitation variability in subseasonal timescales. Given the frequent occurrence of observed KWs, some mechanisms must exist to amplify and maintain KWs to overcome frictional dissipation. Such maintenance mechanisms of KWs are not fully understood, despite the potential influence of KWs on subseasonal forecasts (e.g., Dias et al. 2023) and the tropical rainfall extremes (e.g., Cheng et al. 2023).

Previous observational and modeling studies have proposed two primary maintenance mechanisms of KWs. The first mechanism emphasizes that KWs are *internally* driven by the thermodynamic feedback between diabatic heating and temperature of the KWs, which generates eddy available potential energy (EAPE) within KWs (e.g., Lindzen 1974; Mapes 2000; Straub and Kiladis 2003a; Khouider and Majda 2006; Raymond and Fuchs 2007; Kuang 2008; Chien and Kim 2023). These studies hypothesize that the positive internal thermodynamic feedback occurs within either the first or second baroclinic mode structure, highlighting the importance of deep convection and stratiform processes in maintaining KWs, respectively.

Meanwhile, other studies found that KWs could be *externally* forced by the momentum forcing originating from the midlatitude Rossby waves, which generate eddy kinetic energy (EKE) within KWs (e.g., Hoskins and Yang 2000; Straub and Kiladis 2003b; Tulich and Kiladis 2021; Cheng et al. 2022). As the midlatitude Rossby waves approach the critical latitude in the subtropics (i.e., where the mean westerly wind equals the wave propagation speed), their meridional wavelength shrinks to the minimal, and the waves break. This Rossby wave breaking around the critical latitude exerts momentum on the environment, acting as a transient momentum forcing (Randel and Held 1991). Such momentum forcing remotely amplifies the zonal wind anomalies of KWs.

Despite these insights, the interplay and relative importance of these internal and external mechanisms are not fully understood. As far as we know, Tulich and Kiladis (2021) was the first study that compared the internal and external mechanisms quantitatively. Both the external forcing mechanism and the internal mechanism play significant roles in KW maintenance in their aquaplanet simulations. More recently, Chien and Kim (2024a) quantified the role of the two processes in another set of aquaplanet simulations performed with a different climate model by prescribing sea surface temperature (SST) forcings that mimic the current, a warmer (+4K), and colder (-4K) climates. They concluded that KWs are primarily maintained by the internal thermodynamic feedback in all simulations. While the above discussions on KW maintenance are based on aquaplanet simulations, no studies have specifically quantified the relative importance of the two mechanisms in observations to the best of our knowledge. Because the momentum flux convergence in the aquaplanet simulations is found to be underestimated compared to observations (Chien and Kim 2024), the relative importance of the two maintenance mechanisms in observations may differ from that in the aquaplanet simulations.

The relative importance of the two mechanisms in observations could be a function of region and season, given the pronounced regionality and seasonality in KW characteristics (Roundy and Frank 2004; Yasunaga 2011; Wang and Chen 2016; Chien and Kim 2023; Horng and Yu 2024) and midlatitude Rossby wave activities (Straub and Kiladis 2003b; Huaman et al. 2020; Cheng et al. 2022). For example, Horng and Yu (2024) demonstrated that KWs in the Indian and Pacific basins differ in the relative magnitude of the horizontal advection of moist static energy and the column process. Chien and Kim (2023) found that the internal thermodynamic feedback positively correlates with the underlying SST over the Indo-Pacific warm pool with substantial seasonality. Cheng et al. (2022) showed that KWs in the central Pacific in boreal summer are affected by midlatitude Rossby wave trains from the Southern hemisphere. While past research focused on specific regions and seasons, a systematic overview of the two maintenance mechanisms of KWs across regions and seasons is needed.

This study uses a reanalysis product and satellite observations to quantify the relative importance of the internal and external mechanisms in maintaining KWs in all seasons and regions. The relative importance is quantified by calculating the growth rates of KW eddy available potential energy (EAPE) and eddy kinetic energy (EKE), following Chien and Kim (2024a).

2 Data and Methods

2.1 Data

This study uses two primary datasets: (1) field variables including temperature, zonal wind, meridional wind, vertical velocity, and geopotential obtained from the ERA5 reanalysis (Herbach et al. 2020) at 27 vertical levels from 1000 to 100 hPa and (2) the satellite-observed cloud brightness temperature data same as in Dias et al. (2017). The cloud brightness temperature data is calibrated, combining datasets from the Cloud Archive User Service (CLAUS) (Hodges et al., 2000) and the globally merged infrared radiation (Janowiak et al., 2001). Additionally, ERA5 precipitation is used to characterize the convective activities of KWs and to ensure consistency with diabatic heating. ERA5 variables and cloud brightness temperature are regridded onto 2.5-degree resolution and trimmed to 16 years from 1998 to 2013, with a 3-hourly temporal resolution.

We also analyze climatological SST from the HadISST dataset (Rayner et al. 2003) and zonal wind from ERA5 because they modulate the internal thermodynamic feedback and external momentum forcing (e.g., Straub and Kiladis 2003b; Tulich and Kiladis 2021; Cheng et al. 2022; Chien and Kim 2023),. The mean state zonal wind is calculated from 10-20˚N/S over the winter hemisphere for JJA and DJF (i.e., southern hemisphere for JJA, northern hemisphere for DJF) and both hemispheres for MAM and SON. The choice of the averaging hemisphere is justified (Text S1).

2.2 KW composite

The KW composite characterizes each field associated with the KW's convective lifecycle (i.e., suppressed to enhanced convection). The composite method is adapted from Nakamura and Takayabu (2022), summarized as follows (more details in Text S2): The phase of KW convection is determined by the space-time-filtered cloud brightness temperature anomalies, retaining anomalies within the canonical spectral band of KWs (i.e., 2.5-20 days, wavenumber 1-14, and equivalent depth 8-90m, following Wheeler and Kiladis 1999). The KW phase ranges from $-\pi$ to π. The phases $-\pi/2$ and $\pi/2$ correspond to the most active and suppressed phases of KWs, respectively.

Based on the location of the maximum KW convective variability averaged between 10˚S-10˚N, the KW composite is constructed separately for four domains in the tropics (Fig S1a-b): Africa (345-55˚E, AFR), Indian Ocean (55-130˚E, IO), Western and Central Pacific (130-250˚E, WP-CP), and Eastern Pacific and Atlantic Ocean (250-340˚E, EP-ATL). For each region, the KW composite is also constructed separately for four seasons: December-February (DJF), March-May (MAM), June-August (JJA), and September-November (SON).

Figure S2a shows the number of active KW snapshots used for the KW. Among all seasons, more KWs occur in MAM in most regions (WP-CP, EP-ATL, and AFR), and fewer KWs occur in JJA in EP-ATL and AFR. Similarly, the KW amplitude of cloud brightness temperature and precipitation is higher during MAM in all regions (Fig. S2b-c). While the KW amplitude of cloud brightness temperature presents little regionality (Fig. S2b), the KW amplitude of precipitation is substantially weaker in AFR than in the other regions (Fig. S2c). We suspect the relatively weak KW precipitation variability in AFR is likely because the convective systems there tend to produce more non-precipitating anvil clouds than those in the other tropical regions (e.g., Cetrone and Houze 2009; 2011).

2.3 EAPE and EKE growth rates

The growth rates of EAPE and EKE are quantified to better understand KW convective characteristics. The generation of EAPE and EKE within KWs was first quantified and compared in aquaplanet simulations in Tulich and Kilaids (2021). Later, Chien and Kim (2024a) revised their method and focused on the EAPE (EKE) generation normalized by the total EAPE (EKE) (a.k.a, the growth rate of EAPE or EKE). The EAPE and EKE growth rates serve as a proxy for the growth rates of KWs. Specifically, since the thermodynamic (temperature) and kinematic (zonal wind) fields both exist within KWs, the EAPE and EKE growth rates estimate how fast the thermodynamic and kinematic fields of KWs would grow individually via the internal thermodynamic feedback and external momentum forcing, respectively. Following Chien and Kim (2024a), the EAPE growth rates are calculated based on KW composite diabatic heating (Q) and temperature (T) anomalies separately for the first and second baroclinic vertical modes:

$$\sigma_{EAPE_i} = \frac{\overline{Q_{i,KW} \times T_{i,KW}}}{0.5 \times \overline{T_{i,kw}^{\ 2}}}, \qquad i = 1 \ or \ 2, \tag{1}$$

where i represents each vertical mode, the subscript KW represents KW composite field variables. Diabatic heating is obtained from the residual of the temperature budget (Yanai 1973). The EKE growth rates are calculated based on KW composite momentum flux convergence (F) and zonal wind (U) anomalies for the two baroclinic modes:

$$\sigma_{EKE_i} = \frac{\overline{F_{i,KW} \times U_{i,KW}}}{0.5 \times \overline{U_{i,KW}^{\ 2}}}, \qquad i = 1 \ or \ 2. \tag{2}$$

The momentum flux convergence is obtained from the momentum budget following Cheng et al. (2022). The residual of the momentum budget is negligible in ERA5 reanalysis (Text S6). The relative importance of the internal and external processes in maintaining KWs is quantified by the relative magnitude of EAPE and EKE growth rates.

While Chien and Kim (2024) used the empirical orthogonal function (EOF) approach to obtain the first and second baroclinic structures (details in Text S3), this study takes the analytical approach that was developed by Fulton and Schubert (1985) and adapted in Haertel (2020). We briefly described the method here (more details can be found in Tulich et al. 2007 and Haertel et al. 2008). The analytical vertical model decomposition represents solutions to linear equations of motion for a compressible atmosphere in hydrostatic balance as a superposition of modes, each of which is isomorphic to a solution of shallow water equations for a particular equivalent depth. With rigid lid boundary conditions on vertical velocity at the bottom and top of the troposphere, we obtain eigenfunctions that represent vertical structures and the corresponding eigenvalues that represent the theoretical phase speeds for each structure. Practically, we use the vertical profile of the basic state temperature to obtain the first and second baroclinic modes for wind as the eigenfunctions. The first (second) baroclinic mode for temperature is derived from the corresponding first (second) baroclinic mode of zonal wind under the hydrostatic balance approximation. Our first and second baroclinic mode structures are similar to previous studies (e.g., Trenberth 2000; Haertel and Kiladis 2004; Tulich et al. 2007; Haertel 2020). Note that we also diagnosed the EAPE and EKE growth rates based on empirical vertical mode decomposition, following Chien and Kim (2024). Results are qualitatively similar (details in Text S9).

3 Results

3.1 The geographical and seasonal characteristics of KWs

To explore the geographical and seasonal variation of KW convection (Fig. S1, S2), Figure 1a shows the amplitude of the KW composite diabatic heating (shading) and momentum flux convergence (blue contour), determined by the average of the maximum and the minimum of each field over the entire KW lifecycle. The amplitude of KW diabatic heating generally follows the mean SST (Fig. 1p), with distinct major peaks in IO, WP, and ATL. Two weaker peaks of KW diabatic heating occur near 240˚E and 30˚E, where the nearby SST is low (Fig. 1p). In the upper troposphere, the momentum flux convergence collocates with a robust mean westerly (Fig. 1a, grey contour). The momentum flux convergence is nearly zero in IO, while it is more evident in WP-CP to the east of the dateline (180˚E), the Eastern Pacific, and over the Eastern Atlantic and Africa (near 0˚E). Overall, the KW diabatic heating is strongest in IO and weakest in AFR (Fig. 1b), consistent with KW precipitation (Fig. S2c), while the momentum flux convergence is strongest in WP-CP and EP-ATL, and weakest in IO (Fig. 1c). We speculate that weak KWs near 240˚E and 30˚E are likely enhanced by the momentum flux convergence aloft despite low SST.

Among all seasons, KW diabatic heating and precipitation are strongest during MAM in most regions (Fig. 1g, Fig. S2c), associated with the higher and more zonally uniform SSTs (Fig. 1p). Conversely, the season of maximum momentum flux convergence varies regionally, with a peak during JJA in EP-ATL (Fig. 1l) and MAM in WP-CP (Fig. 1i). Despite the regionality and seasonality, Figure 1 confirms that both internal thermodynamic feedback and external forcing may affect KW maintenance.

3.2 KW EAPE and EKE growth rates

To investigate the relative roles of the two maintenance mechanisms, Figure 2 shows the global KW composite structures. The global KW composite diabatic heating and temperature anomalies (Fig. 2a) display a westward-tilted feature and show robust evolution with increasing KW phase, from suppressed convection, congestus, deep convection, to stratiform processes, consistent with the canonical KW structure (e.g., Kiladis et al. 2009). The first baroclinic warm (cool) anomalies overlap more with the negative (positive) diabatic heating, contributing to the negative EAPE growth rate of the first baroclinic mode (-3.28/day) (Fig. 2c). Figure 2d shows that the first baroclinic mode EAPE growth is generally negative for all regions and seasons, with some magnitude differences (Text S4), associated with the corresponding magnitudes of KW diabatic heating (Fig. S3-7). The first baroclinic mode EAPE growth negatively correlates with KW amplitude in precipitation (Text S5).

Conversely, the second baroclinic mode heating and temperature are positively correlated in the global KW composite (Fig. 2g), contributing to the positive EAPE growth rate of the second baroclinic mode (5.31/day). The second baroclinic mode EAPE growth rate is also positive in all seasons and across the entire tropics (Fig. 2h), with some variations in the magnitude (Text S4). The second baroclinic mode EAPE growth rate positively correlates with KW amplitude in cloud brightness temperature (Text S5), likely because the cloud brightness temperature within KWs is affected mainly by the second mode of diabatic heating. Overall, the negative first-baroclinic-mode EAPE growth rate and the positive second-baroclinic-mode EAPE growth rate in all regions and seasons are consistent with previous results from reanalyses (Chien and Kim 2023) and aquaplanet simulations (Chien and Kim 2024a).

The global KW composite momentum flux convergence anomalies (Fig. 2b, shading) are most substantial in the upper troposphere, where the KW zonal wind anomalies peak (Fig. 2b, contours), suggesting that the momentum flux convergence would likely amplify zonal wind (e.g., Tulich and Kiladis 2021; Cheng et al. 2022; Chien and Kim 2024a). This positive correlation between zonal wind and momentum flux convergence exists in both the first baroclinic component (Fig. 2e) and the second baroclinic component (Fig. 2i), leading to positive EKE growth rates of the first (0.50/day) and second (0.42/day) modes. Figures 2f and 2j show that the EKE growth rates of both modes are positive in nearly all seasons and regions, except that the first baroclinic mode EKE growth is negative in the IO in JJA.

The EKE growth rates of the first (Fig. 2f) and second (Fig. 2j) modes show similar regionality and seasonality. Among all regions, IO has the weakest EKE growth rate for both modes, consistent with the weaker momentum flux convergence in IO (Fig. 1a&c). Among all seasons, the EKE growth rate in EP-ATL is most substantial during JJA, consistent with the stronger momentum flux convergence (Fig. 1l, 2f). Similarly, the EKE growth of the second baroclinic mode in WP-CP is fastest during MAM due to stronger momentum flux convergence of the second baroclinic mode (Fig. S5f). The KW amplitude poorly correlates with EKE growth rates for the two baroclinic modes (Text S5), suggesting that external feedback may not dominate the maintenance of KWs.

Overall, compared to the magnitude of the EAPE growth (Fig. 2d&h), the EKE growth rates for both modes are lower (Fig. 2f&j). For the first baroclinic mode KW, the damping of EAPE is very strong compared to the small EKE growth (Fig. 2d&f). This suggests that if the dynamics of the first baroclinic mode KW dominates, KWs are externally driven but strongly damped. However, for the second baroclinic mode KW, the EAPE and EKE generation are positive, but the magnitude of EAPE growth is much larger than that of EKE (Fig. 2h&j). This suggests that if the dynamics of the second baroclinic mode KW dominates, KWs are generated from internal thermodynamic feedback and amplified by external forcing. Although the first and second baroclinic modes both exist in the observed KWs, since KWs occur recursively, we conjecture that they are more likely a growing mode instead of a damped mode. That is, the maintenance of KWs is likely explained by the EAPE and EKE generation associated with the second baroclinic mode. Therefore, we quantify the relative importance of internal feedback and external forcing for amplifying KWs by comparing the second baroclinic mode's EAPE and EKE growth rates. Note that Text S8 explains the prominent first baroclinic signal of the KWs despite strong damping.

The second-baroclinic-mode EAPE growth rate (5.31 day^{-1}) is at least one order of magnitude larger than the second-baroclinic-mode EKE growth rate (0.42 day^{-1}) globally. For each region and season, the magnitude of the EAPE growth rates of the second baroclinic mode (Fig. 2h) is also higher than that of the EKE growth rate (Fig. 2j). While some seasonal and regional variations exist, the internal thermodynamic feedback is the dominant mechanism that maintains KWs in most seasons and basins (Fig. 2).

Our results slightly differ from those of Tulich and Kiladis (2021). In their aquaplanet simulations, the EKE production within KWs is comparable to EAPE production when vertically integrated (their Fig. 7a). While they showed the amount of EKE and EAPE production [W m^{-2}], we showed their growth rates [s^{-1}], to focus on the rate of time changes instead of the absolute magnitude (Eqs. 1 and 2). However, our EAPE and EKE production terms without normalization show qualitatively similar results (Fig. S10). Another possible reason for the discrepancy between our results and theirs is that the position and strength of the upper tropospheric westerly jet differ, caused by different surface boundary conditions (aquaplanet vs. full geography).

3.3 Environmental modulation of KW EAPE and EKE growth rates

Figure 3a quantifies the relative importance of internal feedback and external forcing using the ratio of EKE and EAPE growth rates associated with the second baroclinic mode. The ratio of EKE growth to EAPE growth (the EKE-to-EAPE ratio hereafter) ranges from 2% to 38%, depending on the regions and seasons. Among all regions, the annual EKE-to-EAPE ratio is the lowest in the Indian Ocean (2.6%) and higher in AFR (14.2%), EP-ATL (12.7%), and WP-CP (7.9%). Seasonally, the EKE-to-EAPE ratio is largest during JJA in EP-ATL (38.5%). The regionality and seasonality of the EKE-to-EAPE ratio are mainly determined by the EKE growth rate (Fig. 2j). Note that we also diagnosed the EAPE and EKE growth rates based on empirical vertical mode decomposition following Chien and Kim (2024). Results are qualitatively similar, except that external momentum forcing is slightly less important in EP-ATL in JJA (details in Text S9).

The EKE-to-EAPE ratio negatively correlates with the mean state SST (Fig. 3b) and positively correlates with the mean state upper tropospheric zonal wind at 200 hPa (U200) (Fig. 3c); similar results are found between 100 and 300 hPa. IO has the smallest EKE-to-EAPE ratio with the highest SST and the weakest upper-level westerly (orange symbols). Conversely, the largest EKE-to-EAPE ratio occurs in EP-ATL and AFR, with stronger upper-level westerly and lower SST (blue and magenta symbols). In WP-CP, the EKE-to-EAPE ratio is slightly lower than that in EP-ATL and AFR, which may be associated with moderate SST (green symbols).

In summary, while KW convective characteristics display distinct peaks in IO, WP-CP, EP-ATL, and AFR (Fig. S1-2), the partition of the internal feedback and external forcing varies as KWs travel globally, depending on the mean SST and U200 locally.

4 Conclusions

This study examined the relative importance of internal thermodynamic feedback and external momentum forcing in maintaining KWs, quantified by the EAPE and EKE growth rates associated with the two baroclinic modes. Results showed that KWs are maintained primarily by the internal thermodynamic feedback in most seasons and basins: the internal thermodynamic feedback amplifies KWs at least four times faster than the external momentum forcing does. Our results support the hypothesis posited by Straub and Kiladis (2003b) that KWs can grow spontaneously without the persistence of extratropical forcing.

Although the internal thermodynamic feedback dominates in the first order, the relative importance of the two maintenance processes varies considerably with regions and seasons. The internal thermodynamic feedback is the most important in the Indian Ocean, where the warmest sea surface temperature favors strong convection and enhances the feedback. Meanwhile, the weakest upper tropospheric mean westerly limits midlatitude waves approaching the tropics. As KWs travel eastward over the Eastern Pacific, Atlantic Ocean, and Africa, the mean westerly aloft strengthens, which enhances the amplification of KWs due to stronger external momentum forcing. The extratropical effect on African KWs has been relatively less emphasized in previous literature, which focused on the midlatitude influence over the Atlantic and Pacific oceans (e.g., Straub and Kiladis 2003b; Liebmann et al. 2009; Mayta et al. 2021; Cheng et al. 2022). Regarding seasonality, the external forcing in the Eastern Pacific, the Atlantic Ocean, and Africa is relatively more important during JJA.

Overall, this study provides an observational baseline on the relative importance of the two maintenance processes for KWs, which can be compared with KWs in model simulations. As many global climate models struggle to represent KW amplitude realistically (e.g., Lin et al. 2006), quantifying the relative contribution of the internal feedback and external forcing to KW maintenance in climate models would provide valuable insights. Meanwhile, diverse representations of KWs are found in convectively-resolved and parameterized simulations, especially in the KW diabatic heating and the moisture-precipitation relationship (e.g., Weber et al. 2021; Rios-Berrios et al. 2023; Lee et al. 2025). As more and more global and near-global cloud-resolving simulations are available nowadays (e.g., Stevens et al. 2019), it is worthwhile to compare the internal thermodynamic feedback within KWs in simulations with resolved or parameterized convection.

Regarding future projection of KWs, using aquaplanet simulations under zonally symmetric SST with uniform surface cooling and warming, Chien and Kim (2024a) found that KWs weaken with warming due to the weakening of internal thermodynamic feedback, while the external feedback plays a minimal role. Oppositely, based on the sixth version of coupled model intercomparison project (CMIP6) simulations, Bartana et al. (2022) found that KWs strengthen with warming. They hypothesized that the projected increase in the intensity of KWs could be due to the changes in extratropical influence. The discrepancies in the future projection of KW characteristics and their mechanisms found in the recent studies warrant an in-depth analysis of the future changes of internal thermodynamic feedback and external momentum forcing under more realistic (e.g., zonally asymmetric) SST boundary conditions.

It is worth noting that our analysis focuses on the indirect effect of the extratropical forcing on KWs, rather than the direct effect of extratropical forcing on ‘eastward-propagating disturbance’ mentioned in previous studies (e.g., Cheng et al. 2022; Huaman et al. 2020; Knippertz 2007). Those ‘eastward-propagating disturbances’ have similar dispersion relationships with the KWs, while their dynamical structures resemble the extratropical cloud plumes. Our study shows consistent dynamical structures as the canonical KWs, suggesting the extratropical cloud plumes do not dominate our results (Text S7 for more details). Additionally, our study focuses on the nonlinear effect of extratropical forcing on KWs based on the resonance between momentum flux convergence and zonal wind anomalies. We do not explicitly account for the linear effect of KW-forced subtropical gyre that feedback to the KW itself, mentioned in previous studies (e.g., Roundy 2008; Tulich and Kiladis 2021; Matthews et al. 2021; Barpanda et al. 2023; Holube et al. 2024). Future research can quantify this linear effect and compare it with the nonlinear effect in this study.

Acknowledgments

This work is part of the first author's PhD dissertation. DK was funded by the New Faculty Startup Fund and Creative-Pioneering Researchers Program from Seoul National University, the National Research Foundation of Korea (NRF) grant funded by the Korea government (MSIT) (RS-2024-00336160), NOAA CVP program (NA22OAR4310608), NOAA MAPP program (NA21OAR4310343), and NASA MAP program (80NSSC21K1495). We appreciate Dr. Stefan Tulich's extensive scientific feedback during peer review and Prof. Peter Blossey's help in improving the writing. We also acknowledge Dr. Juliana Dias, Dr. Naoko Sakeada, Dr. Kazyuoshi Kikuchi, Dr. George Kiladis, and Dr. Maria Gehne for providing the CLAUS dataset.

Open Research

The data and analysis code are publicly available on Zenodo (Chien and Kim 2024b, DOI: 10.5281/zenodo.14026979).

References

Barpanda, P., Tulich, S. N., Dias, J., & Kiladis, G. N. (2023). The role of subtropical rossby waves in amplifying the divergent circulation of the madden–julian oscillation. *Journal of the Atmospheric Sciences*, *80*(10), 2377-2398, https://doi.org/10.1175/JAS-D-22-0259.1

Bartana, H., Garfinkel, C. I., Shamir, O., & Rao, J. (2022). Projected future changes in equatorial wave spectrum in CMIP6. *Climate Dynamics*, 1-13, https://doi.org/10.1007/s00382-022-06510-y

Cetrone, J., & Houze Jr, R. A. (2009). Anvil clouds of tropical mesoscale convective systems in monsoon regions. *Quarterly Journal of the Royal Meteorological Society: A journal of the atmospheric sciences, applied meteorology and physical oceanography*, *135*(639), 305-317, https://doi.org/10.1002/qj.389

Cetrone, J., & Houze, R. A. (2011). Leading and trailing anvil clouds of West African squall lines. *Journal of the atmospheric sciences*, *68*(5), 1114-1123, https://doi.org/10.1175/2011JAS3580.1

Charney, J. G., 1963: A note on large-scale motions in the tropics. *J. Atmos. Sci.*, **20**, 607–609.

Cheng, Y. M., Dias, J., Kiladis, G., Feng, Z., & Leung, L. R. (2023). Mesoscale convective systems modulated by convectively coupled equatorial waves. *Geophysical Research Letters*, *50*(10), e2023GL103335, https://doi.org/10.1029/2023GL103335

Cheng, Y. M., Tulich, S., Kiladis, G. N., & Dias, J. (2022). Two extratropical pathways to forcing tropical convective disturbances. *Journal of Climate*, *35*(20), 2987-3009, https://doi.org/10.1175/JCLI-D-22-0171.1

Chien, M. T., & Kim, D. (2023). Representation of the Convectively Coupled Kelvin Waves in Modern Reanalysis Products. *Journal of the Atmospheric Sciences*, *80*(2), 397-418, https://doi.org/10.1175/JAS-D-22-0067.1

Chien, M. T., & Kim, D. (2024a). Response of convectively coupled Kelvin waves to surface temperature forcing in aquaplanet simulations. *Journal of Advances in Modeling Earth Systems*, *16*(10), e2024MS004378, **https://doi.org/10.1029/2024MS004378**

Chien, M.-T., & Kim, D. (2024b). Maintenance of Convectively Coupled Kelvin waves: Relative Importance of Internal Thermodynamic Feedback and External Momentum Forcing (Code and Data) (CCKW) [Data set]. Zenodo. https://doi.org/10.5281/zenodo.14026979

Dias, J., Gehne, M., Kiladis, G. N., & Magnusson, L. (2023). The role of convectively coupled equatorial waves in Sub-Seasonal predictions. *Geophysical Research Letters*, *50*(21), e2023GL106198, **https://doi.org/10.1029/2023GL106198**

Dias, J., Sakaeda, N., Kiladis, G. N., & Kikuchi, K. (2017). Influences of the MJO on the space-time organization of tropical convection. *Journal of Geophysical Research: Atmospheres*, *122*(15), 8012-8032, **https://doi.org/10.1002/2017JD026526**

Haertel, P. T., & Kiladis, G. N. (2004). Dynamics of 2-day equatorial waves. *Journal of the atmospheric sciences*, *61*(22), 2707-2721, https://doi.org/10.1175/JAS3352.1

Haertel, P. (2020). Kelvin/Rossby wave partition of Madden-Julian oscillation circulations. *Climate*, *9*(1), 2, **https://doi.org/10.3390/cli9010002**

Hersbach, H., and Coauthors, (2020): The ERA5 global reanalysis. Quart. J. Roy. Meteor. Soc., 146, 1999–2049, https://doi.org/10.1002/qj.3803.

Hodges, K. I., D. W. Chappell, G. J. Robinson, and G. Yang (2000), An improved algorithm for generating global window brightness temperatures from multiple satellite infrared imagery, *J. Atmos. Oceanic Technol.*, *17*(10), 1296–1312, https://doi.org/10.1175/1520-0426(2000)017<1296:AIAFGG>2.0.CO;2

Holube, K. M., Lunkeit, F., Vasylkevych, S., & Žagar, N. (2024). Resonant excitation of Kelvin waves by interactions of subtropical Rossby waves and the zonal mean flow. *Journal of the Atmospheric Sciences*, *81*(11), 1833-1848, https://doi.org/10.1175/JAS-D-24-0033.1

Horng, Y. B., & Yu, J. Y. (2024). On the energetics of convectively coupled Kelvin Waves: contrast between Indian and Pacific Basins. *Climate Dynamics*, 1-17, https://doi.org/10.1007/s00382-024-07254-7

Hoskins, B. J., & Yang, G. Y. (2000). The equatorial response to higher-latitude forcing. *Journal of the atmospheric sciences*, *57*(9), 1197-1213, https://doi.org/10.1175/1520-0469(2000)057<1197:TERTHL>2.0.CO;2

Huaman, L., Schumacher, C., & Kiladis, G. N. (2020). Eastward-propagating disturbances in the tropical Pacific. Monthly Weather Review, 148(9), 3713-3728, https://doi.org/10.1175/MWR-D-20-0029.1

Janowiak, J. E., R. J. Joyce, and Y. Yarosh (2001), A real-time global half-hourly pixel-resolution infrared dataset and its applications, *Bull. Am. Meteorol. Soc.*, *82*, 205–217, https://doi.org/10.1175/1520-0477(2001)082<0205:ARTGHH>2.3.CO;2

Kiladis, G. N., Wheeler, M. C., Haertel, P. T., Straub, K. H., & Roundy, P. E. (2009). Convectively coupled equatorial waves. *Reviews of Geophysics*, *47*(2), https://doi.org/10.1029/2008RG000266

Khouider, B., & Majda, A. J. (2006). A simple multicloud parameterization for convectively coupled tropical waves. Part I: Linear analysis. *Journal of the atmospheric sciences*, *63*(4), 1308-1323, https://doi.org/10.1175/JAS3677.1

Knippertz, P. (2007). Tropical–extratropical interactions related to upper-level troughs at low latitudes. *Dynamics of Atmospheres and Oceans*, *43*(1-2), 36-62, https://doi.org/10.1016/j.dynatmoce.2006.06.003

Kuang, Z., 2008: A moisture-stratiform instability for convectively coupled waves. *J. Atmos. Sci.*, 65, 834–854, https://doi.org/10.1175/2007JAS2444.1.

Lee, S.-H., Park, S.-H., Chien, M.-T., & Kim, D. (2025). Simulations of Convectively Coupled Kelvin Waves (CCKWs) with Three Different Cumulus Parameterization Schemes. *Journal of Geophysical Research – Atmosphere*, https://doi.org/10.1029/2024JD042738

Liebmann, B., Kiladis, G. N., Carvalho, L. M., Jones, C., Vera, C. S., Bladé, I., & Allured, D. (2009). Origin of convectively coupled Kelvin waves over South America. *Journal of climate*, *22*(2), 300-315, https://doi.org/10.1175/2008JCLI2340.1

Lin, J. L., Kiladis, G. N., Mapes, B. E., Weickmann, K. M., Sperber, K. R., Lin, W., ... & Emori, S. (2006). Tropical intraseasonal variability in 14 IPCC AR4 climate models. Part I: Convective signals. *Journal of Climate*, *19*(12), 2665-2690, https://doi.org/10.1175/JCLI3735.1

Lindzen, R. S., 1974: Wave-CISK in the tropics. *J. Atmos. Sci.*, 31, 156–179, https://doi.org/10.1175/1520-0469(1974)031,0156:WCITT.2.0.CO;2.

Mapes, B. E., 2000: Convective inhibition, subgrid-scale triggering energy, and stratiform instability in a toy tropical wave model. *J. Atmos. Sci.*, 57, 1515–1535, https://doi.org/10.1175/1520-469(2000)057,1515:CISSTE.2.0.CO;2.

Matthews, A. J. (2021). Dynamical propagation and growth mechanisms for convectively coupled equatorial Kelvin waves over the Indian Ocean. *Quarterly Journal of the Royal Meteorological Society*, *147*(741), 4310-4336, **https://doi.org/10.1002/qj.4179**

Mayta, V. C., Kiladis, G. N., Dias, J., Silva Dias, P. L., & Gehne, M. (2021). Convectively coupled Kelvin waves over tropical South America. *Journal of Climate*, *34*(16), 6531-6547, https://doi.org/10.1175/JCLI-D-20-0662.1

Nakamura, Y., & Takayabu, Y. N. (2022). Convective Couplings with Equatorial Rossby Waves and Equatorial Kelvin Waves. Part I: Coupled Wave Structures. *Journal of the Atmospheric Sciences*, *79*(1), 247-262, https://doi.org/10.1175/JAS-D-21-0080.1

Randel, W., & Held, I. (1991). Phase speed spectra of transient eddy fluxes and critical layer absorption. *Journal of the atmospheric sciences*, *48*(5), 688-697, https://doi.org/10.1175/1520-0469(1991)048<0688:PSSOTE>2.0.CO;2

Raymond, D. J., and Zˇ . Fuchs, 2007: Convectively coupled gravity and moisture modes in a simple atmospheric model. *Tellus*, 59A, 627–640, https://doi.org/10.1111/j.1600-0870.2007.00268.x.

Rayner, N. A., D. E. Parker, E. B. Horton, C. K. Folland, L. V. Alexander, D. P. Rowell, E. C. Kent, and A. Kaplan, 2003: Global analyses of sea surface temperature, sea ice, and night marine air temperature since the late nineteenth century. J. Geophys. Res., 108, 4407, https://doi.org/10.1029/2002JD002670.

Roundy, P. E. and W. M. Frank, 2004: A climatology of waves in the equatorial region. *J. Atmos. Sci.*, 61, 2105–2132, https://doi.org/10.1175/1520-0469(2004)061,2105:ACOWIT.2.0.CO;2.

Roundy, P. E. (2008). Analysis of convectively coupled Kelvin waves in the Indian Ocean MJO. *Journal of the Atmospheric Sciences*, *65*(4), 1342-1359, https://doi.org/10.1175/2007JAS2345.1

Rios-Berrios, R., Judt, F., Bryan, G., Medeiros, B., & Wang, W. (2023). Three-dimensional structure of convectively coupled equatorial waves in aquaplanet experiments with resolved or parameterized convection. *Journal of Climate*, 36(9), 2895-2915, https://doi.org/10.1175/JCLI-D-22-0422.1

Stevens, B., Satoh, M., Auger, L., Biercamp, J., Bretherton, C. S., Chen, X., ... & Zhou, L. (2019). DYAMOND: the DYnamics of the Atmospheric general circulation Modeled On Non-hydrostatic Domains. *Progress in Earth and Planetary Science*, *6*(1), 1-17, https://doi.org/10.1186/s40645-019-0304-z

Straub, K. H, G. N. Kiladis, 2003a: The observed structure of convectively coupled Kelvin waves: Comparison with simple models of coupled wave instability. *J. Atmos. Sci.*, 60, 1655–1668, https://doi.org/10.1175/1520-0469(2003)060,1655:TOSOCC.2.0.CO;2.

Straub, K. H., & Kiladis, G. N, 2003b. Extratropical forcing of convectively coupled Kelvin waves during austral winter. *Journal of the atmospheric sciences*, *60*(3), 526-543, https://doi.org/10.1175/1520-0469(2003)060<0526:EFOCCK>2.0.CO;2

Trenberth, K. E., Stepaniak, D. P., & Caron, J. M. (2000). The global monsoon as seen through the divergent atmospheric circulation. *Journal of Climate*, *13*(22), 3969-3993, https://doi.org/10.1175/1520-0442(2000)013<3969:TGMAST>2.0.CO;2

Tulich, S. N., Randall, D. A., & Mapes, B. E. (2007). Vertical-mode and cloud decomposition of large-scale convectively coupled gravity waves in a two-dimensional cloud-resolving model. *Journal of the atmospheric sciences*, *64*(4), 1210-1229, https://doi.org/10.1175/JAS3884.1

Tulich, S. N., & Kiladis, G. N. (2021). On the regionality of moist Kelvin waves and the MJO: The critical role of the background zonal flow. *Journal of Advances in Modeling Earth Systems*, *13*(9), e2021MS002528, https://doi.org/10.1029/2021MS002528

Wang, L., and L. Chen, 2016: Interannual variation of convectively coupled equatorial waves and their association with environmental factors. *Dyn. Atmos. Oceans*, 76, 116–126, https://doi.org/10.1016/j.dynatmoce.2016.10.004.

Weber, Nicholas J., Daehyun Kim, and Clifford F. Mass. "Convection–Kelvin wave coupling in a global convection-permitting model." *Journal of the Atmospheric Sciences* 78.4 (2021): 1039-1055, https://doi.org/10.1175/JAS-D-20-0243.1

Wheeler, M., and G. N. Kiladis, 1999: Convectively coupled equatorial waves: Analysis of clouds and temperature in the wavenumber–frequency domain. *J. Atmos. Sci.*, 56, 374–399, https://doi.org/10.1175/1520-0469(1999)056,0374:CCEWAO.2.0.CO;2.

Yasunaga, K., 2011: Seasonality and regionality of the Madden-Julian oscillation and convectively coupled equatorial waves. *SOLA*, 7, 153–156, https://doi.org/10.2151/sola.2011-039.

Figures

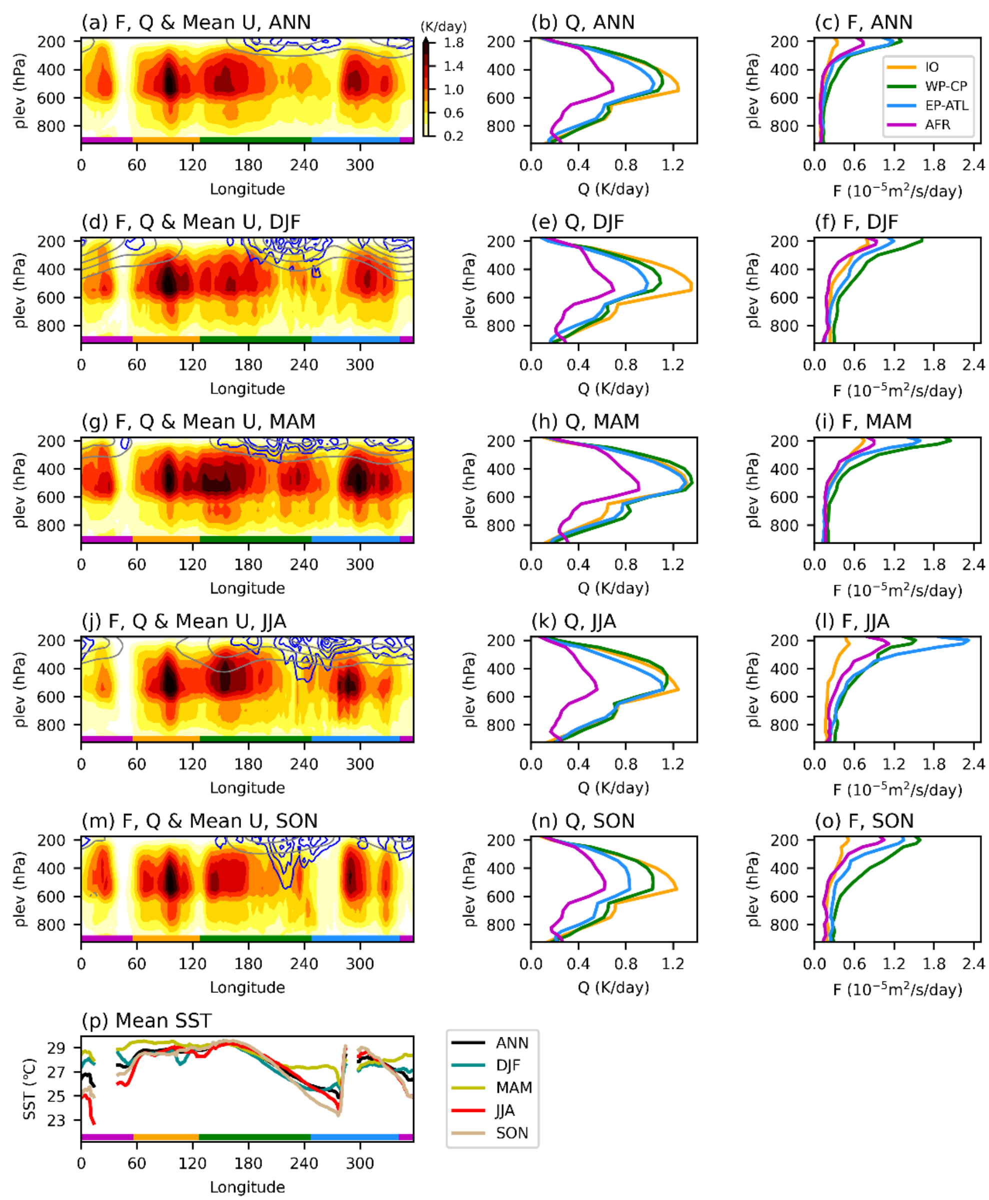

Figure 1. (a) The amplitude of diabatic heating (shading) and momentum flux convergence anomalies (blue contour) within KWs and the mean state zonal wind (grey contour) in all months. Zonal wind is only shown for the upper troposphere (< 500 hPa). (b) The amplitude of diabatic heating anomalies within KWs averaged over each region: Africa (purple), Indian Ocean (orange), Western and Central Pacific (green), Eastern Pacific, and Atlantic Ocean (light blue). (c) Similar to b, but showing the amplitude of momentum flux convergence averaged over each

region. (d-f) Same as a-c, but in DJF. (g-i) Same as a-c, but in MAM. (j-l) Same as a-c, but in JJA. (m-o) Same as a-c, but in SON. (p) The mean state sea surface temperature averaged over 10˚S-10˚N.

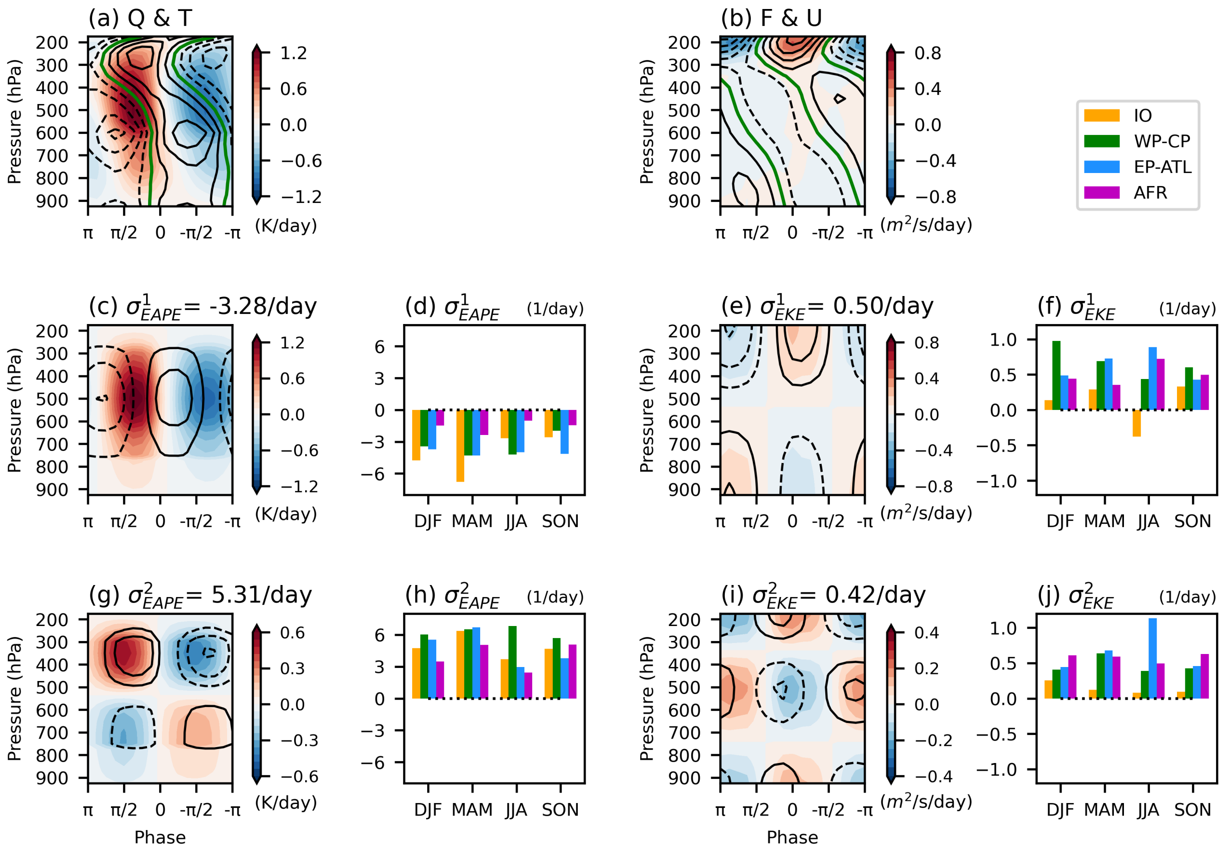

Figure 2. (a) Total KW vertical structure of diabatic heating and temperature anomalies. (b) Total KW vertical structure of momentum flux convergence and zonal wind anomalies. The total fields are decomposed into the first (c, e) and second (g, i) baroclinic mode components. (d) The first baroclinic mode EAPE growth rate for each region and season. (e) The first baroclinic mode EKE growth rate for each region and season. (h) The second baroclinic mode EAPE growth rate for each region and season. (j) The second baroclinic mode EKE growth rate for each region and season.

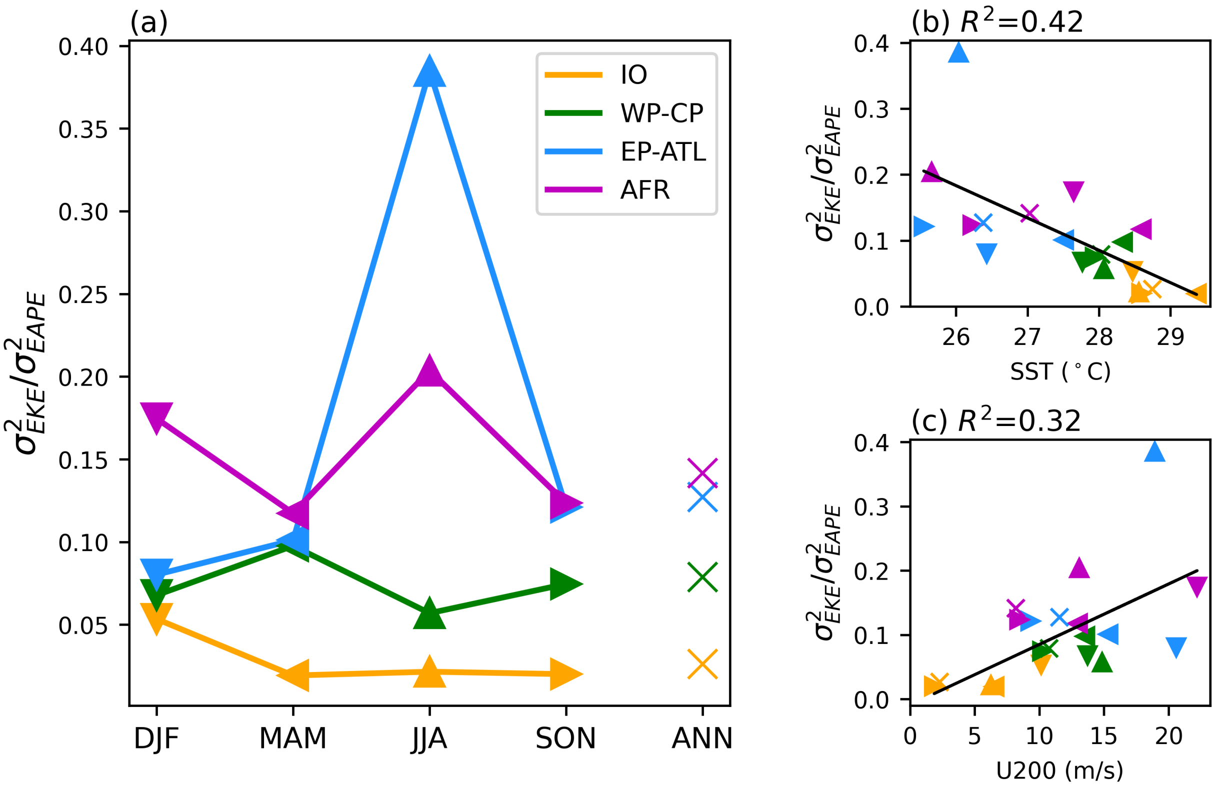

Figure 3. (a) The relative importance of EKE to EAPE growth for the second baroclinic mode for each region and season. (b) The ratio of the second baroclinic mode EKE to EAPE growth rate and the mean state sea surface temperature (SST), (c) The ratio of the second baroclinic mode EKE to EAPE growth rate and zonal wind at 200 hPa (U200). The linear regression lines are indicated in black. The triangles pointing downward represent DJF, leftward represent MAM, upward represent JJA, and rightward represent SON. The annual mean is shown in crosses.

Geophysical Research Letters

Supporting Information for

Maintenance of Convectively Coupled Kelvin Waves: Relative Importance of Internal Thermodynamic Feedback and External Momentum Forcing

Mu-Ting Chien[1,2], Daehyun Kim[1,3], & Patrick Haertel[4]

[1]Department of Atmospheric and Climate Sciences, University of Washington

[2]Department of Atmospheric Science, Colorado State University

[3]School of Earth and Environmental Sciences, Seoul National University, South Korea

[4]School of Earth and Planetary Sciences, Yale University

Contents of this file

Text S1 to S9
Figures S1 to S16

Introduction

The supporting information contains eight text sections and fifteen figures supplementary to the main results.

Text S1. Justification for the choice of mean state variables and the pre-processing of the upper tropospheric zonal wind

The climatological sea surface temperature and zonal wind in the upper troposphere are the main mean state variables analyzed in this study. The two variables are chosen based on previous studies, which found that internal thermodynamic feedback is stronger when sea surface temperature (SST) is high (e.g., Chien and Kim 2023) and that the stronger external feedback collocates with strong westerly in the upper troposphere (e.g., Cheng et al. 2022).

The upper tropospheric zonal wind of the mean state is averaged over 10-20˚N/S over the winter hemisphere for JJA and DJF (i.e., southern hemisphere for JJA, northern hemisphere for DJF), and both hemispheres for MAM and SON. The choice of winter hemisphere for JJA and DJF is supported by previous studies which showed that KWs in boreal summer in the Central Pacific are related to the midlatitude wave trains from the southern hemisphere (e.g., Straub and Kiladis 2003b; Cheng et al. 2022), while KWs in eastern Pacific in DJF are associated with the midlatitude wave trains from the northern hemisphere (e.g., Huaman et al. 2020; Cheng et al. 2022). Note that the collocation of momentum flux convergence and the upper tropospheric westerly is less obvious if averaging over both hemispheres (not shown).

Text S2. KW composite method

The anomalies of all variables are calculated by first removing the annual mean, the first three harmonics of the annual cycle, and the 30-day low-pass filtered variability and then projecting the resulting anomalies onto the KW meridional structure (the meridional structure that maximizes at the equator and decays exponentially with latitude). For temperature, diabatic heating, and zonal wind, we ensure only the signals within 10˚S to 10˚N are projected, whereas for the momentum flux convergence, to emphasize the source from the midlatitude waves, we exclude the signals within 10˚S to 10˚N. The meridionally projected anomalies are composited based on the KW convective phase obtained from the KW-space-time-filtered cloud brightness temperature. The KW-space-time filtering retains signals within the KW band (Wheeler and Kiladis 1999), corresponding to zonal wavenumber 1-14, period 2.5-20 days, and equivalent depth 8-90 m. Note that the method above closely follows previous studies (Tulich and Kiladis 2021; Cheng et al. 2022; Chien and Kim 2024a).

The KW composite is done by averaging over thousands of the 3-hourly snapshots with active KWs (i.e., KW convective signal greater than one standard deviation). The number of active KW snapshots for each region and season is shown in Fig. S2a. We also do the KW composite for each longitude with a window of 10 degrees of longitude centered around each longitude to further investigate the longitudinal structure of KWs (Fig. 1). Amplitudes of each KW composite field used in Fig. 1 for each pressure level are obtained by the average between the magnitude of the maximum and minimum values of the KW composite fields.

Text S3. Obtain the first and second baroclinic modes using empirical approach

The first and second baroclinic modes for diabatic heating and temperature are obtained from the empirical orthogonal functional (EOF) analysis of diabatic heating anomalies for supplementary materials. The vertical structure of the first baroclinic mode diabatic heating and temperature shows a single sign across the whole troposphere with a maximum in the midtroposphere, while the second baroclinic mode shows a dipole structure with peaks in the upper and lower troposphere (e.g., Haertel and Kiladis 2004; Tulich et al. 2007).

To ensure dynamical consistency between the vertical modes of diabatic heating and zonal wind, the first and second baroclinic modes for zonal wind and momentum flux convergence are obtained from the vertical derivation of the vertical structure of the pressure vertical velocity (omega), where the vertical structure of omega is derived from the EOF of diabatic heating normalized by static stability under the strict weak temperature gradient approximation (Charney 1963). The first baroclinic mode wind structure shows a dipole across the whole troposphere. In contrast, the second baroclinic mode wind structure exhibits three layers of positive and negative anomalies across the troposphere, consistent with the corresponding circulation of the diabatic heating structure (e.g., Trenberth et al. 2000; Tulich et al. 2007). Ten passes of a 1-2-1 filter are applied to the two vertical modes of diabatic heating (temperature) and zonal wind (momentum flux convergence) for smoothness. Note that more details of this method can be found in Chien and Kim (2024).

Text S4. The geographical and seasonal variation of EAPE and EKE growth rates

The first baroclinic mode EAPE appears to experience the strongest damping in IO and the weakest damping in AFR in DJF and MAM, associated with the strongest and weakest diabatic heating in IO and AFR, respectively (Fig. 1b, S3b). In terms of seasonality, the first baroclinic mode EAPE damping is strongest in MAM in most regions (IO, WP-CP, and AFR).

Among all regions, the second baroclinic mode EAPE growth rate shows a stronger growth in IO, WP-CP, and EP-ATL (Fig. S3c). In comparison, slightly weaker growth is observed in AFR (Fig. S3c). In terms of the seasonality, as with the EAPE growth of the first baroclinic mode, the magnitude of the second baroclinic mode EAPE growth rate is largest during MAM in most regions (IO, EP-ATL, and AFR), due to stronger diabatic heating (Fig. 1h, S4c, S6c, S7c). The second baroclinic mode EAPE growth is weaker during JJA in AFR due to weaker diabatic heating (Fig. 1k, Fig. S6c).

On the other hand, the seasonality of the EKE growth rate for the second baroclinic mode in AFR is small, consistent with the small seasonality of the amplitude of momentum flux convergence (Fig. 1f, i, l, o). However, a slightly weaker growth of the second baroclinic mode EKE occurs in JJA (Fig. 2j, Fig. S6f).

Text S5. Correlation between KW amplitude and the EAPE and EKE growth rates

The first baroclinic mode EAPE growth negatively correlates with KW amplitude, especially KW amplitude in precipitation (Fig. S8d). The first baroclinic mode EKE growth rate has little correlation with KW amplitude in cloud brightness temperature and precipitation (Fig. S8b, e). The KW amplitude in precipitation and cloud brightness temperature correlate positively (Fig. S8c). On the other hand, the second baroclinic mode EAPE growth is positively correlated with KW amplitude in cloud brightness temperature and precipitation (Fig. S9a, d). The EKE growth rate of the second baroclinic mode also has nearly zero correlation with KW amplitude in cloud brightness temperature and precipitation (Fig. S9b, e). Because the correlation between KW amplitude and EKE growth is small, the correlation between KW amplitude and the EKE-to-EAPE ratio is also small, mostly determined by the opposite sign of the correlation between the EAPE growth rate and KW amplitude. These suggest that the EAPE growth within the second baroclinic mode is likely the most dominant mechanism for maintaining KWs.

Text S6. Momentum budget residual analysis

We diagnosed the residual term in the momentum budget in ERA5 reanalysis following Cheng et al. (2022). The method is summarized below:

$$Residual = \frac{\partial u'}{\partial t} - F' - Linear\_terms,$$

$$Linear\_terms = u'\frac{\partial \bar{u}}{\partial x} - v'\frac{\partial \bar{u}}{\partial y} - \omega'\frac{\partial \bar{u}}{\partial p} - \bar{v}\frac{\partial u'}{\partial y} - \bar{\omega}\frac{\partial u'}{\partial p} + fv' - \frac{\partial \phi'}{\partial x}.$$

Some manipulation of the equations above yields

$$\frac{1}{2}\frac{\partial u'^2}{\partial t} = u'(Linear\_terms) + u'F' + u'(Residual).$$

We then project the linear terms, F', residual, and u' on Kelvin-mode meridional structure. Then, we composite each meridionally projected term with respect to KW phase. Afterwards, we calculated the projection of each KW composite term to the KW composite u' to obtain the contribution of each term to KW maintenance (similar to Fig. 10b in Cheng et al. 2022). The contribution of each term to KW maintenance is calculated as follows:

$$Sm = \frac{\| u_p' x_p' \|}{\| u_p' u_p' \|},$$

where x_p corresponds to each meridionally projected KW composite term from the momentum budget, including linear terms, F', and residual. "|| ||"denotes the average over the entire KW lifecycle.

Figure S11 shows the contribution of each term in the momentum budget to KW maintenance in each region for all seasons. We found that the residual in the momentum budget is negligible in most regions, except that in the Indian Ocean, the contribution of residual is comparable to other terms.

Text S7. Extratropical cloud plumes vs. KWs

The extratropical cloud plumes identified by Cheng et al. (2022) and Huaman et al. (2020), which show different dynamical structures to convectively coupled Kelvin waves (KWs), are restricted to a specific domain over the Eastern Pacific Ocean (180-280°E, 15°S-20°N). Figure 12 by Cheng et al. (2022) showed that the Q vector mainly occurs north of 10°N in boreal winter in East Pac and that the cloud signals of extratropical cloud plumes almost exclusively occur poleward of 10°N. However, KWs analyzed in our study are restricted to those with cloud signals within 10°S-10°N and with larger amplitude near the equator (given that we apply Kelvin-wave-meridional projection to all fields). Furthermore, the zonal extent of where the extratropical cloud plumes are identified in Cheng et al. (2022) (180-280°E) is mostly covered by our Western and Central Pacific domain (130-250°E) and partially covered by our Eastern Pacific and Atlantic Ocean (250-345°E). Since our zonal and meridional extent of the domain is different from the domain of the extratropical cloud plumes found in Cheng et al. (2022) and Huaman et al. (2020), the extratropical cloud plumes are unlikely to dominate the KW composite results in our study. Instead, our analysis is dominated by the real KW signal.

With our regional definition, our KW composite results show dynamical structures that are consistent with the canonical understanding of convectively coupled Kelvin waves in previous studies (e.g., Kiladis et al. 2009) and different from extratropical cloud plumes. A few KW characteristics we find different from extratropical cloud plumes are as follows (we will show our results from Western and Central Pacific, Eastern Pacific, and Atlantic for demonstration, but a similar conclusion can be drawn for all regions and seasons in our study):

1. The KW composite zonal wind anomalies in the upper and lower troposphere are in opposite signs and westward-tilted, suggesting the existence of the first and second baroclinic modes (Fig. S12, left). This differs from the extratropical cloud plumes that show strong upper-level zonal wind but weak lower-level zonal wind, and the zonal wind anomalies are eastward-tilted in the vertical (Fig. S12, right).

2. The KW composite momentum flux convergence F and zonal wind anomalies u are positively correlated in the upper troposphere in our analysis (Fig. S12, left). On the other hand, F and u in quadrature for extratropical cloud plumes in Cheng et al. (2022) (Fig. S12, right).

The above argument is also valid for EP-ATL and AFR over boreal winter and spring in our analysis (Fig. S4, S6). Therefore, our analysis is also not affected significantly by the extratropical cloud plumes mentioned in Knippertz (2007).

Text S8. Why is the first baroclinic mode KW prominent, given a strong damping effect?

Our results suggest that the first-mode signal is an overall damped mode that can be excited by external forcing. Given that the first mode is a damped mode, one reason that the first-mode signal is prominent within KWs is likely because it is a response of the second baroclinic mode dynamics, instead of being responsible for the energy generation of the KWs. For example, in simple models of KWs, such as those in Kuang (2008) and Mapes (2000), the first baroclinic mode is a response to the changes in the second baroclinic mode temperature anomalies. Changes in the second baroclinic mode temperature anomalies either reduce convective inhibition or perturb the quasi-equilibrium states of the lower troposphere, thereby triggering deep convection (first baroclinic heating). The first baroclinic mode temperature anomalies respond to the first baroclinic mode heating, but with a significant lag (damping effect). In other words, although the first baroclinic mode heating damps the first baroclinic mode temperature anomalies, the EAPE generation from the second baroclinic mode heating and temperature anomalies triggers the first baroclinic mode anomalies, and thus, the first-mode signal is still prominent.

Text S9. EAPE and EKE growth rates from the empirical orthogonal function approach following Chien and Kim (2024) vs. the analytical approach from Fulton and Schubert (1985)

Although we take the analytical approach for vertical mode decomposition in the main results, we also conducted the analyses in this paper using the empirical orthogonal function (EOF) approach from Chien and Kim (2024) and found the main results qualitatively similar.

The vertical mode decomposition from Fulton and Schubert compared to EOF is shown in Fig. S13. The analytical approach takes the mean state temperature (Fig. S13a) as the only input to obtain vertical modes of the kinematic fields (i.e., zonal wind and momentum flux convergence) (Fig. S13b, dashed line) and the thermodynamic fields (i.e., temperature and diabatic heating) (Fig. S13c, dashed line) with rigid lid boundary conditions at 175 hPa and 1000 hPa. The first baroclinic modes are shown in red, and the second baroclinic modes are shown in blue. Dashed red and blue lines in Fig. S13 show the first and second baroclinic structures used in the main figures of the paper, which are obtained from the analytical approach. The structures from the EOF analysis (solid lines) and the analytical approach (dashed lines) show qualitatively similar structures, although the nodal point and the maximum of each mode are slightly shifted.

We do not expect the empirical and analytical approaches to yield identical vertical structures because the two approaches are based on different assumptions. The empirical approach finds the dominant structures that explain the largest variance of the diabatic heating anomalies, which directly reflect the dominant cloud processes and their associated wind circulations. The analytical approach finds the vertical structures of the horizontal wind anomalies under hydrostatic balance, with a no-penetrating upper boundary condition, using just a 1-D basic state temperature profile. Since the horizontal wind structure can be linked with the structure of vertical velocity, previous studies also found that the analytical vertical modes can be associated with cloud processes (e.g., Haertel et al. 2008). These suggest that the empirical and analytical approaches emphasize different aspects. However, we find that the analytical approach is more suitable for our paper because the sum of the first and second baroclinic modes from the analytical approach captures the gross vertical structures of KWs better (Fig. S14b, d). That is, significantly smaller residual in the KW composite temperature, as well as the KW composite zonal wind and momentum flux convergence (Fig. S14c, f). The small residual is similar to the 2-day wave diagnostic in Haertel et al. (2008) (their Fig. 6e).

The KW composite vertical structures of diabatic heating, temperature, zonal wind, and momentum flux convergence are also decomposed into the first and second baroclinic modes based on the analytical approach from Fulton and Schubert (1985) (Fig. 2). Figure 2 shows qualitatively similar results to the results from empirical approach (Fig. S15). In particular, the first baroclinic EAPE growth rate is negative, and the second baroclinic EAPE growth rate is positive in all regions and seasons. The second mode EAPE growth rate is higher in Fig. 2 than in Fig. S15. However, the relative magnitude in different basins and seasons remains similar between Fig. 2 and Fig. S15.

For the KW composite momentum flux convergence and zonal wind, results from the analytical approach in Fig. 2 and results from the empirical approach in Fig. S15 are also qualitatively similar, except that the regional EKE growth rate of the second mode in EP-ATL in JJA is slightly higher than that in Fig. 2.

The relative importance of the EAPE and EKE growth rates of the second baroclinic mode based on the analytical approach is shown in the updated Fig. 3. The results are qualitatively similar to the empirical results (Fig. S16). In an annual average sense (crosses in Fig. 3), the internal thermodynamic feedback plays a more important role in all basins (e.g., less than 20% in Fig. 3 and Fig. S16). The regionality of EAPE to EKE growth is also similar, regardless of the decomposition methods used. The Indian Ocean shows the lowest EKE to EAPE ratio, and the EP-ATL shows the highest EKE to EAPE ratio in JJA, although the magnitude is slightly higher in EP-ATL in JJA in Fig. 3 than in Fig. S16. These suggest that the main finding of this paper (the internal thermodynamic feedback is more important in all basins and seasons) holds regardless of the methods for vertical mode decomposition.

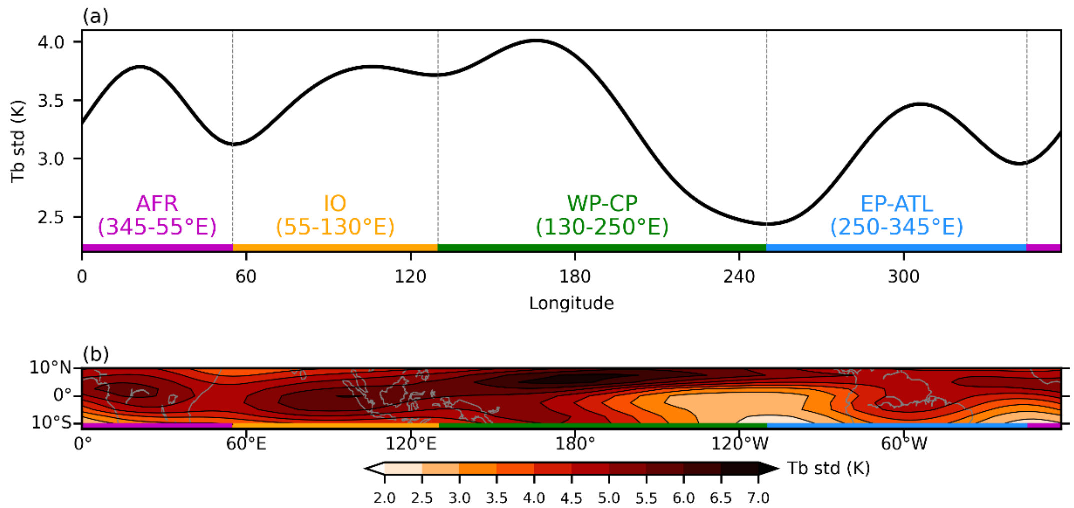

Figure S1. The KW cloud brightness temperature standard deviation in (a) meridional average between 10˚S and 10˚N and (b) horizontal map. Colored horizontal lines in (a) and (b) indicate regional separation used in Fig. 1-3 and Fig. S2-9.

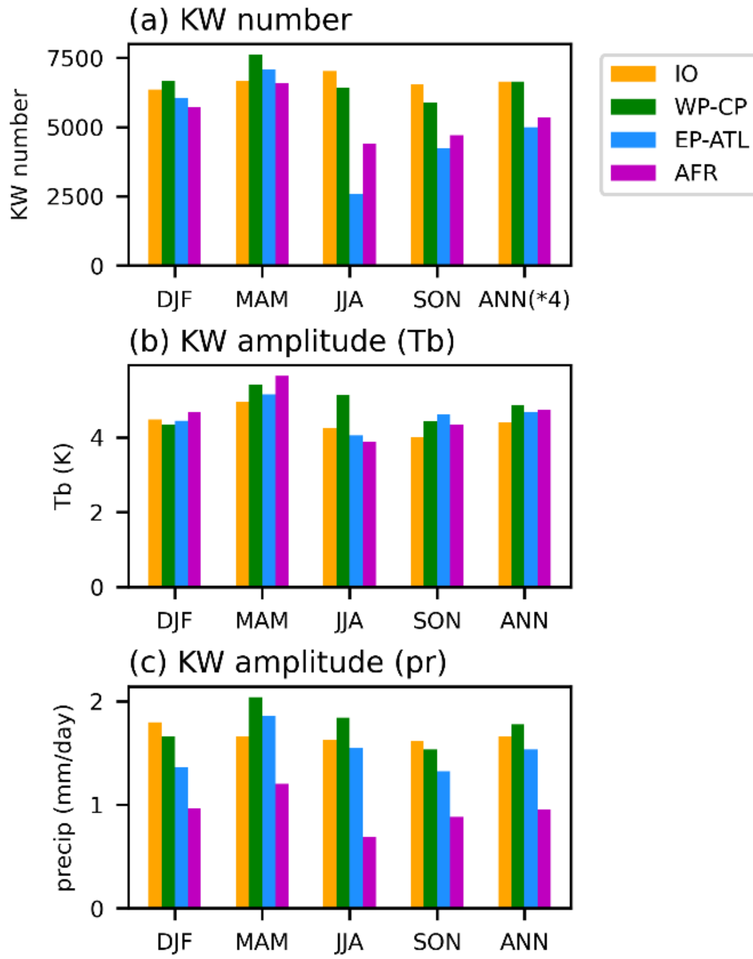

Figure S2. KW statistics for each region and season. (a) Number of snapshots with active KWs, (b) KW amplitude on cloud brightness temperature, and (c) KW amplitude on precipitation. Amplitude is defined as the average of the maximum and minimum signal.

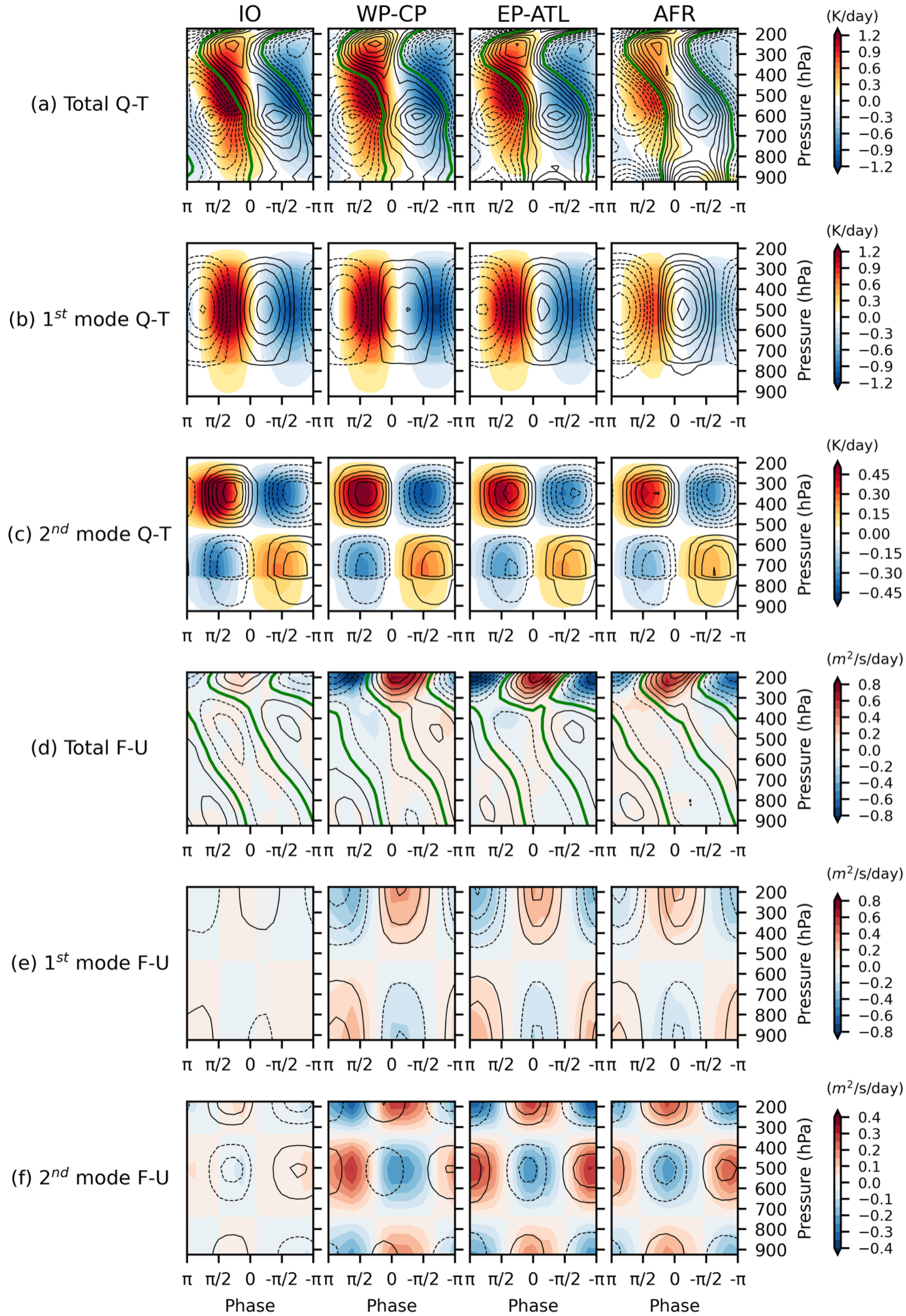

Figure S3. (a-c) Regional KW composite vertical structure of the diabatic heating (shading) and temperature (contour) anomalies: (a) the total, (b) the first baroclinic component, and (c) the second baroclinic component. (d-f) Regional KW composite vertical structure of the momentum flux convergence (shading) and zonal wind (contour) anomalies: (d) the total, (e) the first baroclinic component, and (f) the second baroclinic component.

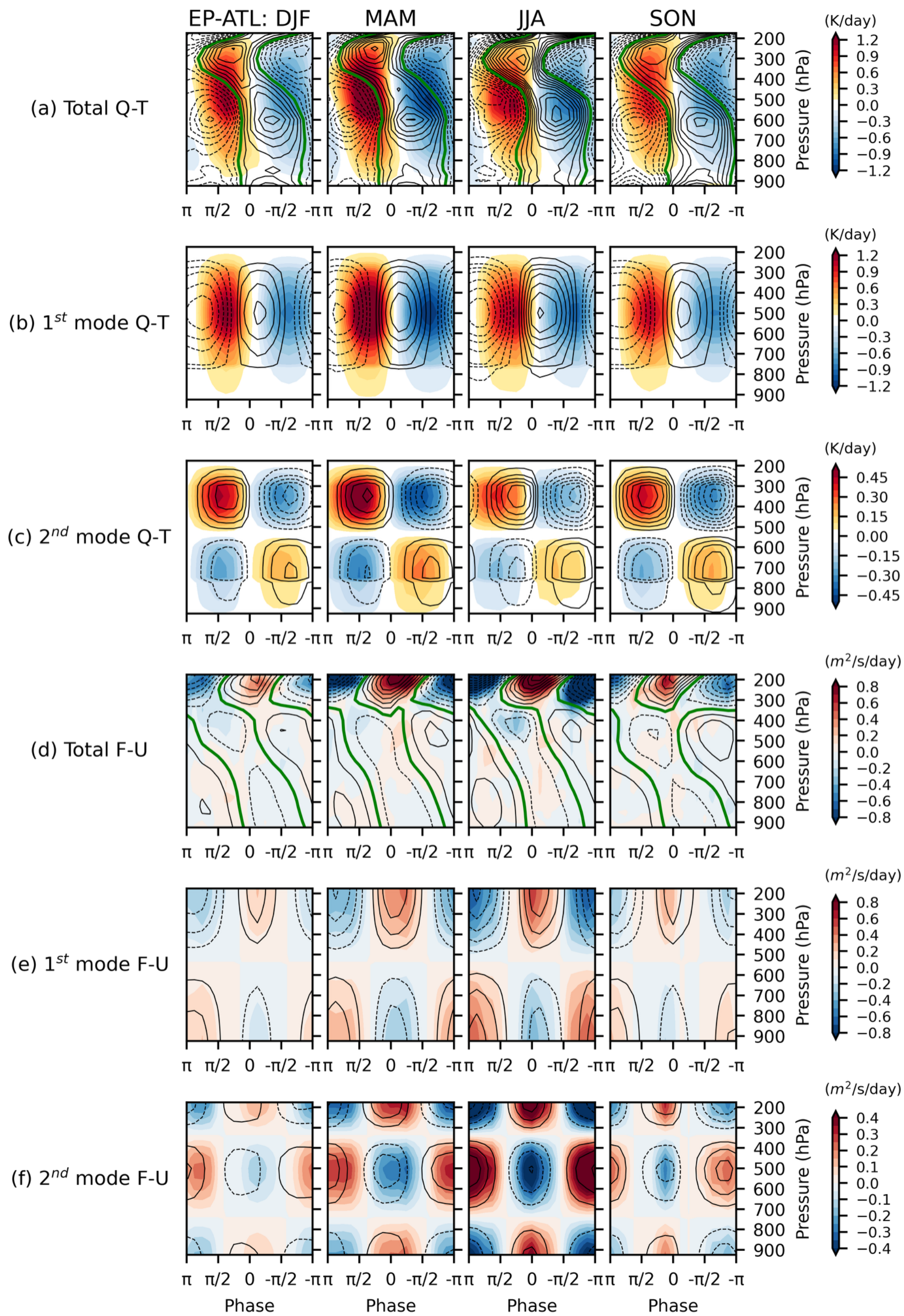

Figure S4. Similar to Fig. S3, but for four seasons in EP-ATL.

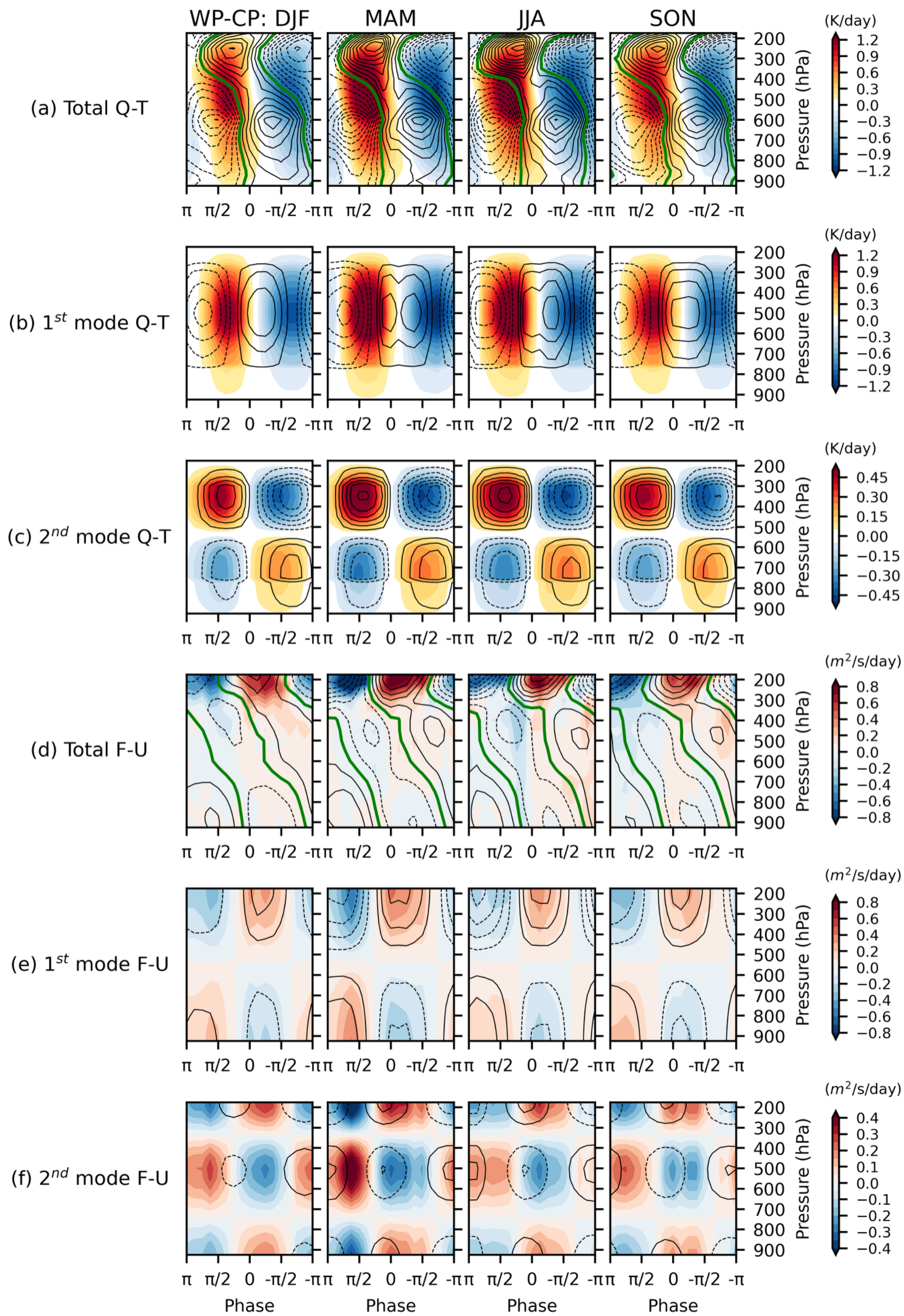

Figure S5. Similar to Fig. S3, but for four seasons in WP-CP.

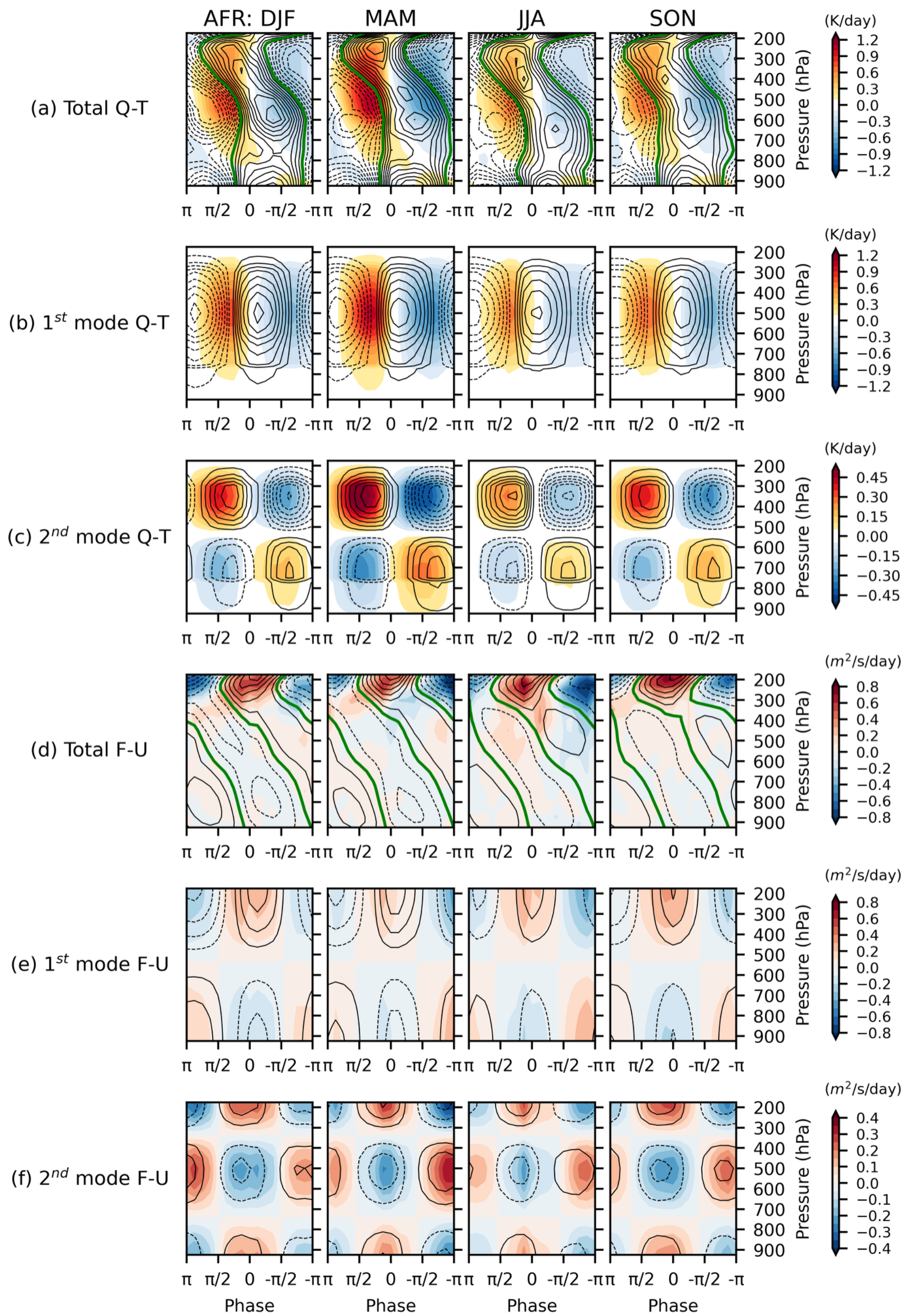

Figure S6. Similar to Fig. S3, but for four seasons in AFR.

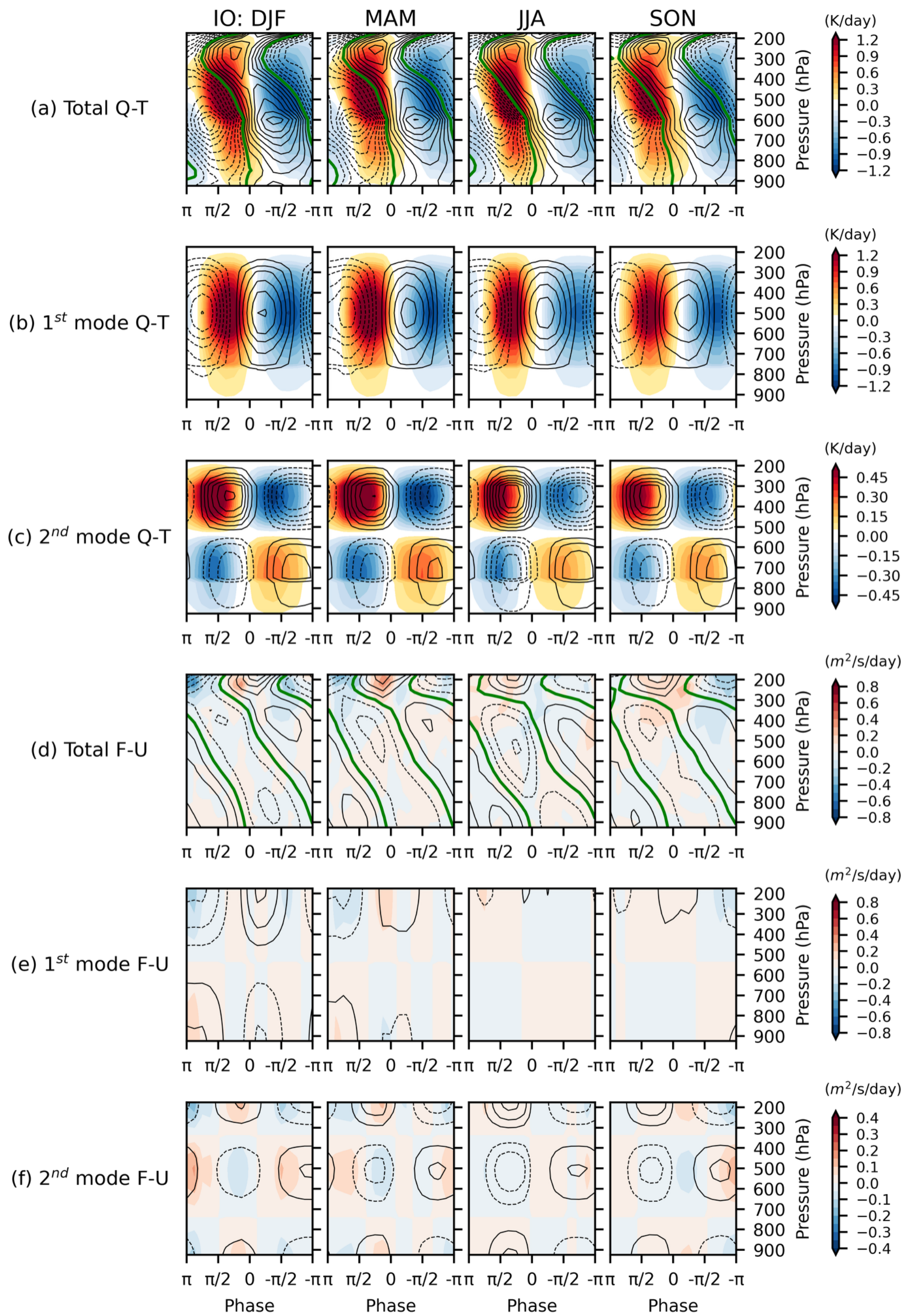

Figure S7. Similar to Fig. S3, but for four seasons in IO.

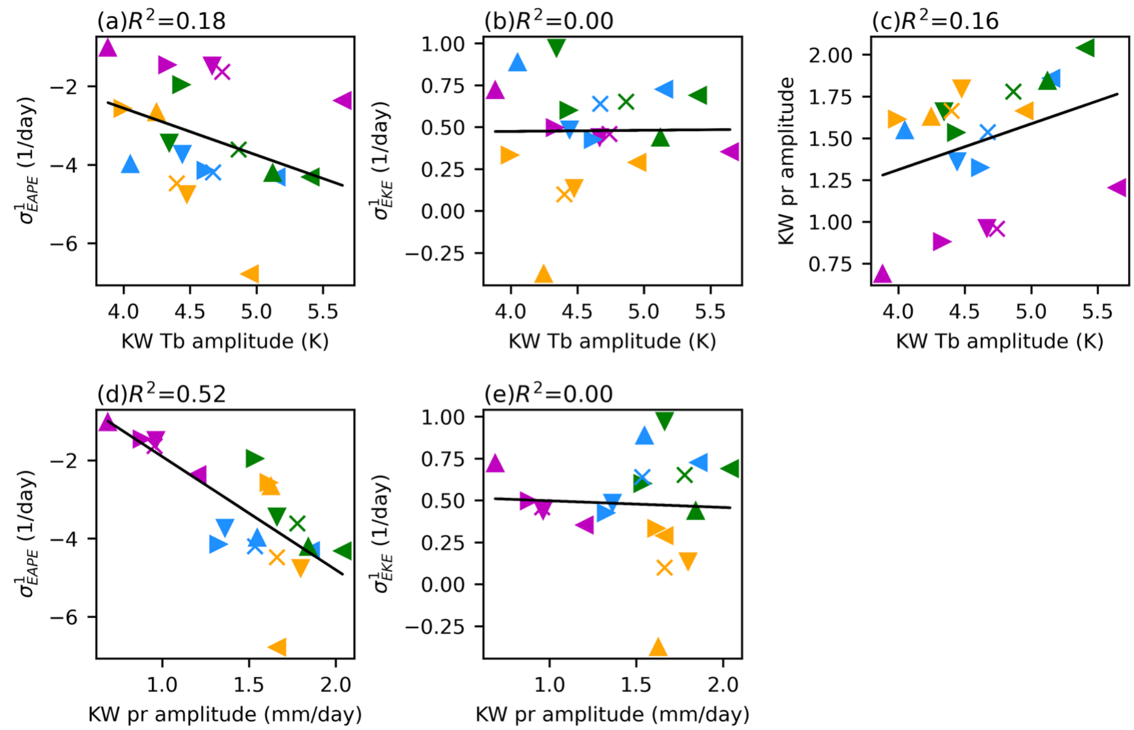

Figure S8. Correlation coefficient between KW amplitude and the EAPE and EKE growth rates of the first baroclinic mode.

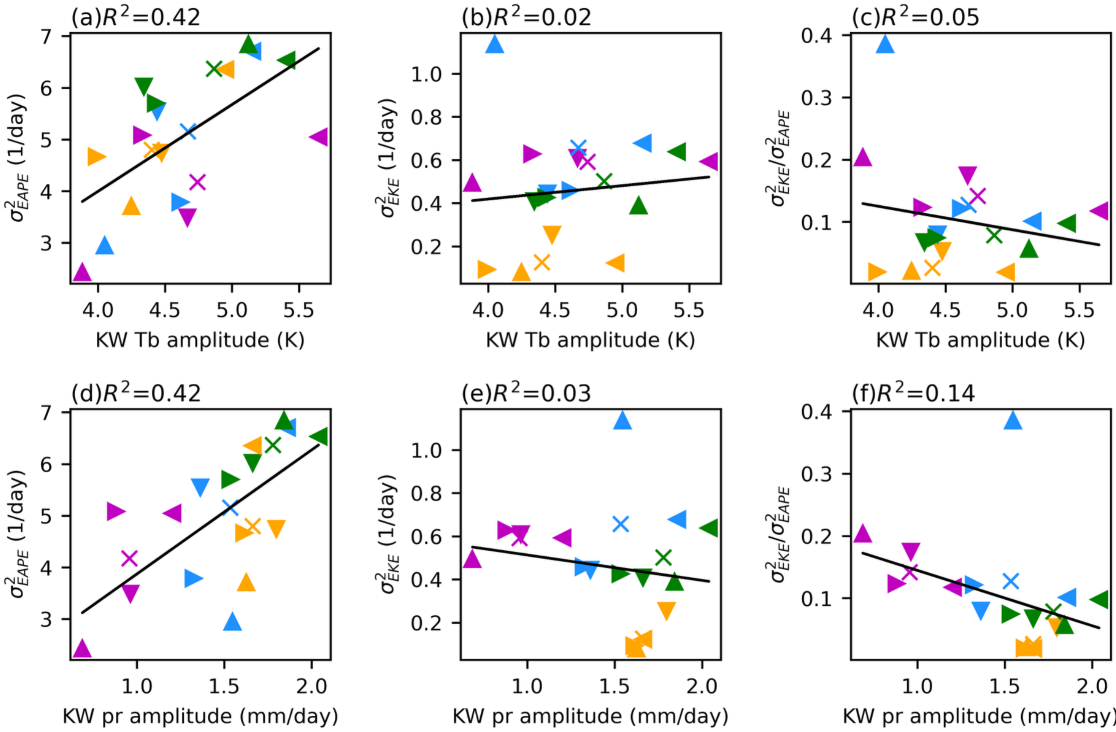

Figure S9. Correlation coefficient between KW amplitude and the EAPE and EKE growth rates of the second baroclinic mode.

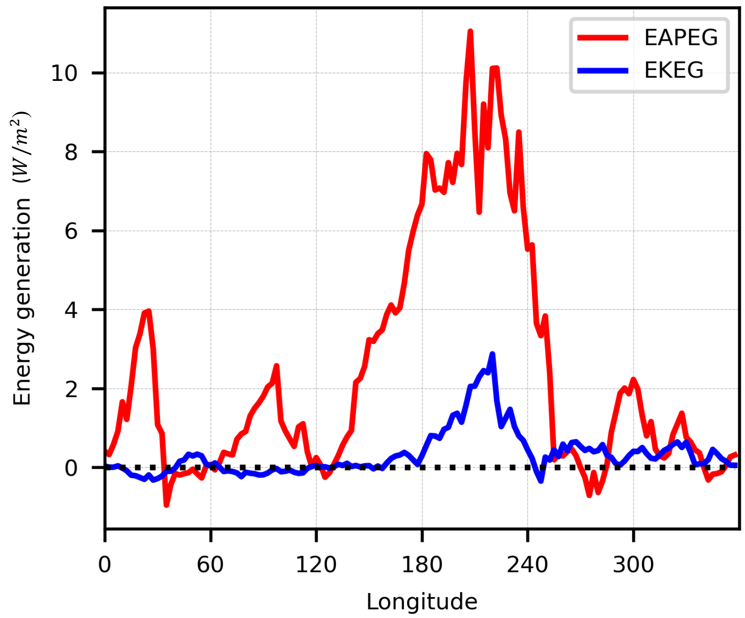

Figure S10. The vertical integration of EAPE (red) and EKE (blue) generation within KWs for each longitude. The energy generation is not normalized.

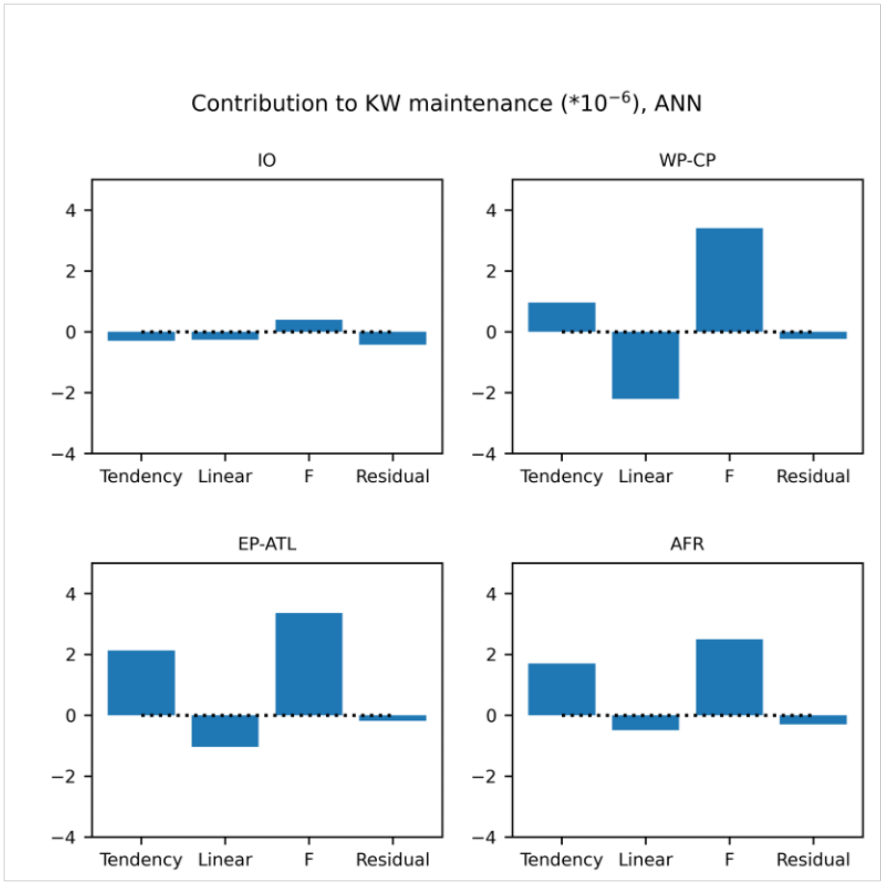

Figure S11. Contribution of each term in the momentum budget to KW maintenance for each region in all seasons.

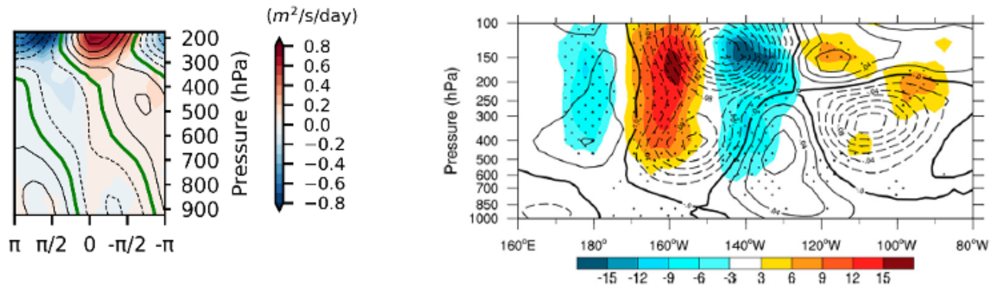

Figure S12. (left) KW composite vertical structure of momentum flux convergence in WP-CP in annual mean from our study (shading) and zonal wind (contour) anomalies in our study. (right) The composite vertical structure of extratropical cloud plumes in Cheng et al. (2022).

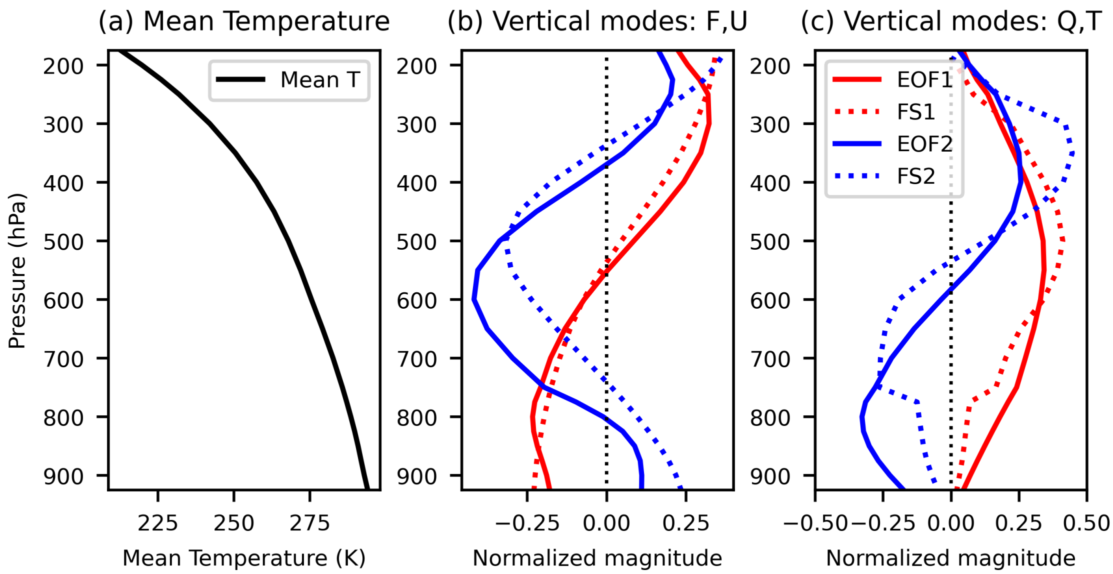

Figure S13. (a) Mean state temperature profile, (b) vertical modes of F and U, and (c) vertical modes of Q and T. Solid lines represent vertical modes form empirical approach in this study (solid line) and dashed lines represent analytical approach following Fulton and Schubert (1985) and Haertel et al. (2020). Red (blue) lines represent the first (second) baroclinic modes.

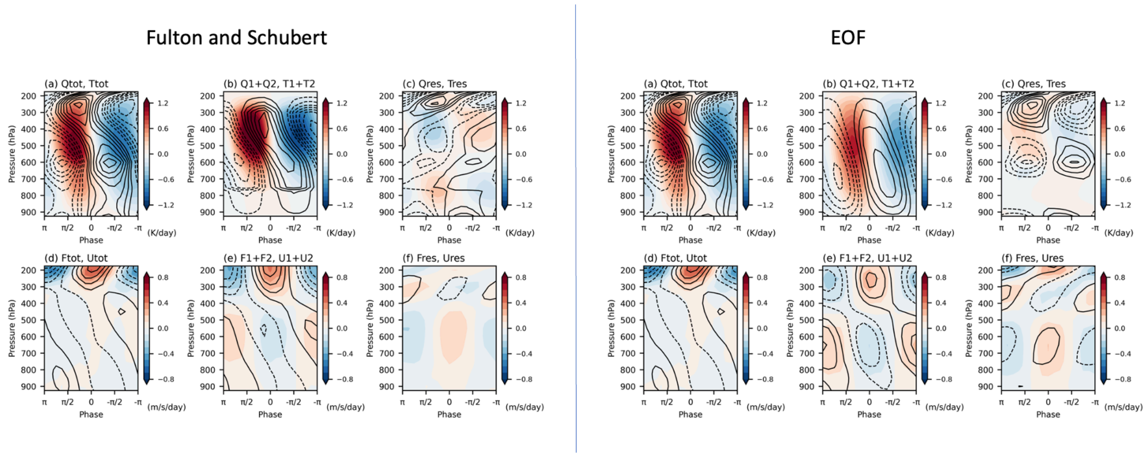

Figure S14. KW composite (a-c) diabatic heating (shading) and temperature (contour) anomalies of the (a) total, (b) first and second baroclinic modes, and (c) residual. KW composite (d-f) momentum flux convergence (shading) and zonal wind (contour) anomalies of the (d) total, (e) first and second baroclinic modes, and (f) residual. Left panels represent the analytical vertical mode decomposition (main results), and right panels show the empirical vertical mode decomposition (supplementary).

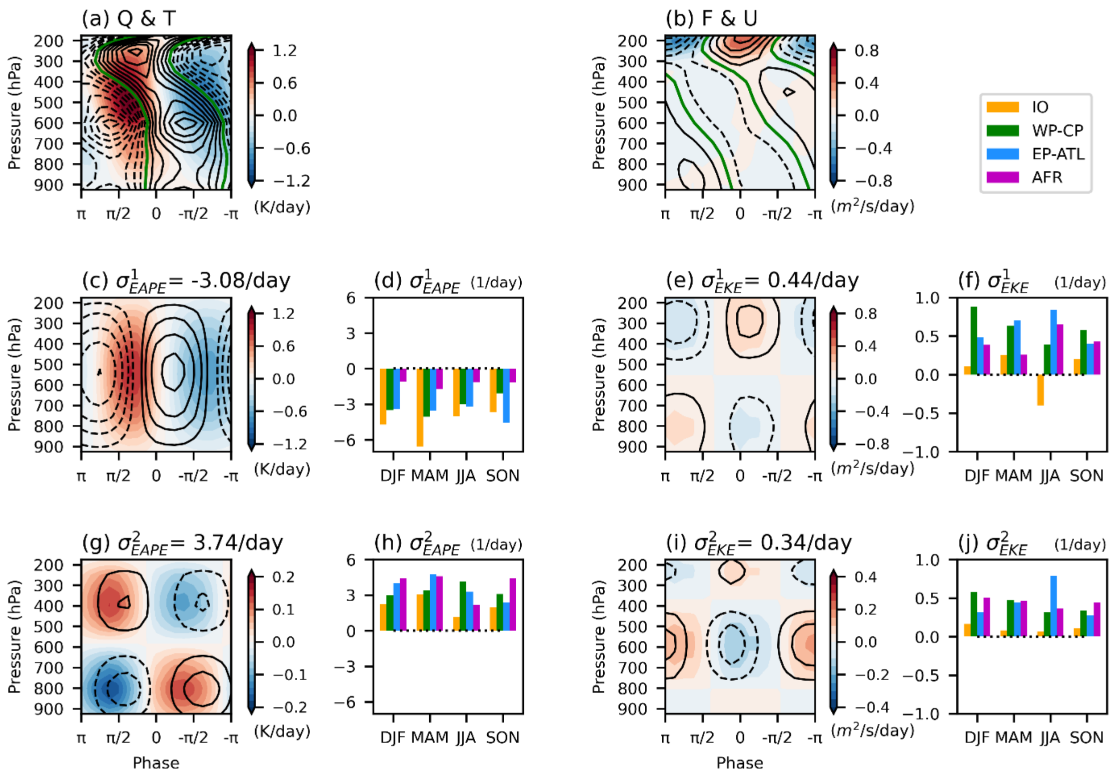

Figure S15. Similar to Fig. 2, but decompose vertical modes empirically following Chien and Kim (2024).

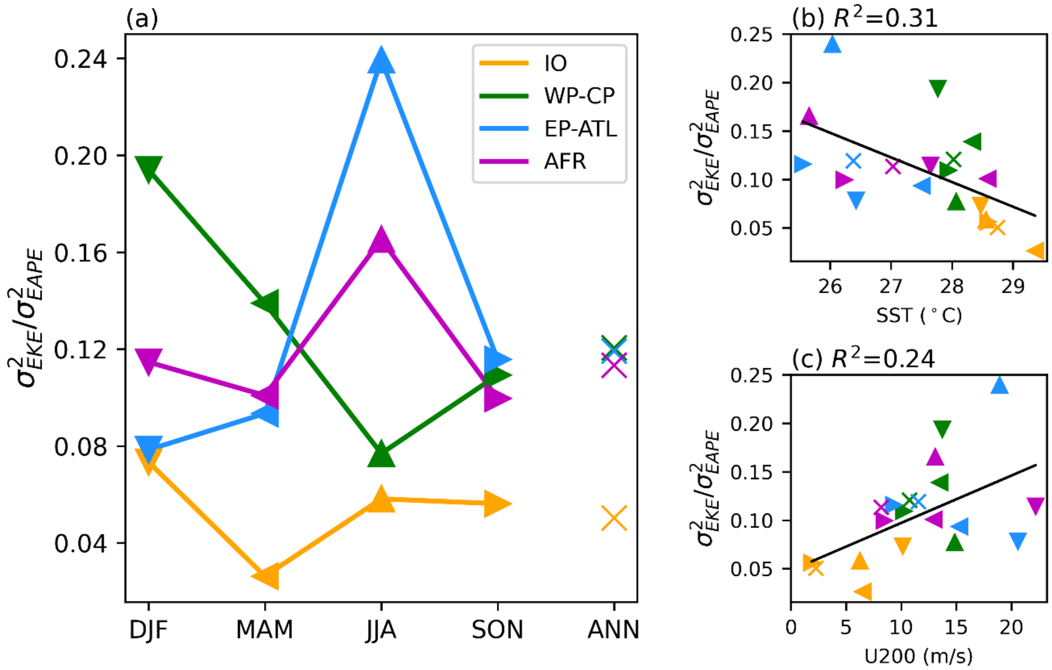

Figure S16. Similar to Fig. 3, but decompose vertical modes empirically following Chien and Kim (2024).